Supplemental Information for "The Temporal and Spatial Distribution of Health, Labor and Agriculture Benefits of Climate Change Mitigation in the US",
Shindell et al., PNAS, doi:10.1073/pnas.2104061118, 2021.

Methods and Additional Analyses

1. Methods

Emissions Scenarios

As described in the main text, we analyzed standard simulations performed for CMIP6 driven by emissions pathways created under the SSP scenarios as well as additional energy-sector decarbonization scenarios (Table S1). The baseline SSPs are intended to span a range of challenge levels for both mitigation and adaptation. They consist of five distinct narratives, referred to as 'Sustainability' (SSP1), 'Middle-of-the-road' (SSP2), 'Regional rivalry' (SSP3), 'Inequality' (SSP4), and 'Fossil-fueled development' (SSP5). For mitigation, challenges are rated as relatively small for SSP1 and SSP4, medium for SSP2, and high for SSP3 and SSP5. Each scenario includes a baseline case as well as additional mitigation scenarios with increasingly stringent climate change mitigation goals. These lead to progressively lower nominal radiative forcing targets (the actual radiative forcing in a climate model can vary substantially from the scenario target) with values that were largely chosen for consistency with the Representative Concentration Pathways (RCPs) developed previously by the scenario community. These scenarios are created using models of the energy-economy-land system that find the least-cost solution to achieving the desired forcing target within the constraints of the storyline, applying policies such as global economy-wide carbon prices or demand mitigation, and hence provide valuable information into the effects of policies to mitigate climate change when applied across all sectors of the economy and in all regions of the world (though not necessarily equally in different places).

In the SSPs, emissions change from all sectors and in all regions, and in response to multiple policies, making it difficult to see the impacts of single policies or actions of single countries. We therefore created addition scenarios that isolate the effects of decarbonization of the energy sector, the single largest contributor to climate change (in part owing to its role in transitioning the transport sector to net-zero via electrification), and implemented those additional scenarios both globally and for the US alone. Our simulations thus allow us to explore the drivers of some of the most significant impacts seen across the SSPs. To create these energy-sector decarbonization scenarios, emissions of all pollutants in the reference "Current Path" case are from the International Institute of Applied Systems Analysis (IIASA) GAINS model, based on their current legislation (CLE) scenario for 2005-2050 (Stohl et al., 2015; IIASA, 2017). This is a trajectory based on existing legislation and energy usage projections from the International Energy Agency (IEA, 2012). The CLE scenario is comparable to the SSP3_70 reference scenario for CO_2. For this project, upon the CLE reference we imposed changes in the energy sector following SSP1 under the very low 1.9 W m^{-2} scenario (SSP1_19) created by the IMAGE model (van Vuuren et al., 2017). For CO_2, for which global totals rather than gridded emissions were provided, the US values are based on the assumption that US emissions are consistent with the

mean trends across OECD nations which is reported in the SSP database. CO_2 emissions from the energy sector in the SSP database are also scaled by 1.06 to match the 2015 values in the CLE scenario as for CO_2, which dominates climate change, it is necessary to match the reference emissions as closely as possible so that the climate differences are solely a result of CO_2 emissions cuts rather than differences between the CLE and SSP1_19 scenario assumptions. In summary, the reference scenario simulated the effects of remaining on a trajectory that accounts for policies that have been enacted into current legislation along with projected changes in energy demand. The first alternate scenario simulated the effects of decarbonizing the US energy sector by 2050 in a manner consistent with the 1.5ºC target of the Paris Climate Agreement. The second alternate scenario simulated the effects of decarbonizing the entire world's energy sector. Only the energy sector is perturbed in our scenarios, so that direct use of energy by industry or in buildings, or energy in transportation are not affected.

For other pollutants, there are sometimes larger mismatches between energy sector emissions in the GAINS model and the IMAGE model as uncertainties are larger (e.g. fugitive methane from the energy sector). These pollutants dominate air quality-related impacts, so our top priority is to match the emissions reductions in the SSP1_19 scenario over time that stem from decarbonization. To maintain comparability with our reference case, these emissions are therefore based on the present-day energy sector emissions from the IIASA GAINS scenario, CLE, taking present-day CLE scaled by the relative change in the SSP1_19 changes in a future year YYYY for the energy sector only (i.e., Emissions in year YYYY are set to CLE(2015) × SSP1_19(YYYY)/SSP1_19(2015)). This methodology allows us to keep the spatial pattern and present-day magnitude for non-CO_2 emissions from the CLE scenario rather than scaling the SSP1_19 emissions to match as was done for CO_2 since they do not have the same spatial patterns in the CLE and SSP1_19 datasets. It also avoids double-counting emissions reductions for many air quality-related pollutants that are already included in the CLE scenario rather than scaling future CLE emissions. This includes 'excess' $PM_{2.5}$ that's largely fly ash from coal as well as traditional $PM_{2.5}$ components. Other sectors follow the CLE reference. We thus include both projected changes in socioeconomics and in energy sector technologies under a 1.9 W m^{-2} scenario.

In the energy sector decarbonization simulations, emissions change through 2050 and are fixed thereafter. The simulations are extended to 2075 to obtain a better indication of the climate response to the emission changes during the first half of the century as climate responds fairly slowly owing to both the decadal and longer timescales of much of the carbon cycle and the slow response of the ocean to greenhouse gas changes. An ensemble of three members is performed for the CLE, US energy sector decarbonization and global energy sector decarbonization scenarios. An ensemble of five members for SSP2_45 is used to characterize uncertainties in all SSP simulations as computational resource limitations prevented the generation of ensembles for the other SSPs. Analyses cover the period 2020-2070 as we use 10 year means centered around each decade's starting year (e.g., 2020, 2030, etc.). For some SSP simulations, daily temperature data was also available out to 2100 and so is used in our valuation analysis. High-resolution air pollution results were not available for the 2070-2100 period, but as rates of change were fairly small or zero towards the end of the simulations through 2070, results for the next decades were extrapolated assuming continuation of those modest changes (if any).

Emissions or concentration scenarios for two key pollutants, NO_x and CO_2, illustrate the behavior of primary drivers of air pollution and climate change, respectively (Figure S1). US emissions of NO_x, an important precursor of both ozone and PM, are projected to decrease substantially in the SSPs explored here with the exception of the high reference SSP5_85. In response to the most aggressive climate change mitigation scenarios SSP1_26 and SSP1_19, reductions are both large and very rapid with cuts of 42 and 56%, respectively, by 2030. These decreases are primarily driven by the large projected decreases from 2020 to 2030 in energy generation from coal (~20%), largely used for power, and from oil (~25%), largely used for transportation, along with modestly improved air pollution controls. Similarly, in the energy-sector decarbonization scenario, US NO_x emissions decrease by 33% by 2030 (starting from a higher baseline (see Methods), hence the use of a distinct reference simulation). The energy-sector decarbonization scenario highlights how that sector's emissions are rapidly reduced under highly ambitious climate change mitigation policies, with minimal changes after 2040 as emissions from that sector reach very low levels. Other aerosol or ozone precursor air pollutants such as SO_2 and CO show fairly similar behavior to that of NO_x. As noted in the main text, surface ozone and aerosol concentrations are essentially synchronous with emissions changes as these pollutants have lifetimes of days to months.

Carbon dioxide concentrations are prescribed in the simulations and are responsive to worldwide emissions. Due to the long atmospheric residence time of CO_2, historical emissions continue to affect future concentrations so that not even the highest ambition scenarios show decreases in CO_2 (despite emissions cuts). For example, projected changes by the year 2070 range from a minimal increase in the SSP1_19 scenario to nearly a doubling in the SSP5_85 scenario (Figure S1). Since CO_2 is a global pollutant, the impact of energy-sector decarbonization in the US only on atmospheric CO_2 concentrations is quite modest even though that sector is fully decarbonized by ~2043. Decarbonization of the energy sector globally, reaching net zero ~2046, contributes greatly to the decrease seen in the SSP1_19 scenario relative to the SSP3_70 reference, however, accounting for roughly 2/3 of the drop in CO_2 emissions. The pace of energy sector CO_2 emissions reductions is slightly faster than that of decarbonization as a whole. Even though the changes in energy sector emissions under a 1.5ºC scenario are greatest in the near-term they affect CO_2 more strongly in the latter half of the century. Other greenhouse gases have distinct projections. In contrast with CO_2, emissions of long-lived N_2O continues to increase in all scenarios, again with a wide range depending upon the level of climate change mitigation and the baseline SSP. This increase in N_2O is because this gas comes mainly from agriculture, and the models do not identify enough mitigation opportunities to compensate for the requirements to provide food to a growing population, combined with the longevity of N_2O. For methane emissions, the range is even broader, extending from a near doubling under the SSP3_70 reference scenario decreases of around 30% by 2070 under SSP1_26 or SSP1_19. Note that the SSPs do not account for possible feedback responses that may change natural methane emissions as a response to climate, though these can be included in climate models.

We analyze changes over time in the simulations, and also compare simulations. For example, we can compare SSP1_19 with SSP3_70. The first set compares a scenario where countries reduce combustion of fossil fuels and take other actions consistent with keeping global warming below 1.5 ºC, which is a goal of the Paris climate agreement, with a reference scenario with only a modest increase in climate mitigation consistent with warming of 4 to 5ºC by the end of the century. Note that in such a comparison across SSP narratives, in this case SSP1 *vs.* SSP3,

differences are due to varied socio-economic trends as well as climate change mitigation policies. In particular the SSP1 envisions a society focused on sustainability, which includes much more than simply decarbonization of energy, for example reduced demand for goods and services with high carbon footprints.

As well as comparing across different SSPs, there is a pair of SSP scenarios that examines a particular policy, namely an emphasis on reducing emissions of near-term climate forcers (methane and precursors of tropospheric ozone and aerosols, also called near-term climate forcers (NTCFs)). Comparison between SSP3_70Low and SSP3_70 thus isolates the impact of policies focused on reductions in NTCF emissions. This represents a highly idealized case consisting of air pollution reduction policies that would reduce emissions of aerosols and aerosol precursors (e.g., scrubbers on coal fired power plants) along with policies to reduce methane emissions, in both cases without affecting CO_2 emissions, and was designed to study climate response rather than provide a plausible policy scenario. Note that a focus on reductions of all near-term climate forcers for the sake of climate mitigation has not been advocated by the community and is largely distinct (except for targeting methane) from suggestions that it would be beneficial to reduce short-lived climate forcers (the warming components within NTCFs) alongside CO_2 reductions as an optimum way to mitigate both near-term and long-term climate change (e.g. Shindell et al., 2012).

Table S1. Scenarios explored in this analysis

Scenario Name	Forcing Target ($W\ m^{-2}$)	Short name	Comments
SSP1- Sustainability	1.9	SSP1_19	
SSP1- Sustainability	2.6	SSP1_26	
SSP2 - Middle-of-the-Road	4.5	SSP2_45	
SSP3 - Regional Rivalry	7.0	SSP3_70	Primary reference case for SSPs
SSP3 - Regional Rivalry	7.0	SSP3_70Low	Low near-term climate forcer emissions
SSP4 - Inequality	3.4	SSP4_34	
SSP4 - Inequality	6.0	SSP4_60	
SSP5 - Fossil-fueled Development	3.4	SSP5_34	Overshoot scenario, i.e. forcing substantially exceeds 3.4 $W\ m^{-2}$ before returning to that level.
SSP5 - Fossil-fueled Development	8.5	SSP5_85	Alternative reference case for SSPs
Current Path or Current Legislation (CLE)		Current Path	Reference for Sectoral Simulations
Global Energy Sector Decarbonization		Decarb Energy Global	CLE except Global Energy sector emissions scaled to follow SSP1_19
US Energy Sector Decarbonization		Decarb Energy US	CLE except US Energy sector emissions scaled to follow SSP1_19

Composition Modeling: Additional Simulations

The GISS-E2.1-G model used in the current Coupled Model Intercomparison Project phase 6 (CMIP6) realistically captures many observed physical quantities and trends (e.g. Kelley et al., 2020; Seltzer et al., 2017). The standard GISS CMIP6 simulations did not use the within grid-box emissions information to alter constituent gradients and provide high resolution $PM_{2.5}$ output (Shindell et a., 2018). We therefore used ozone and temperature data from the CMIP6 SSP simulations, but to obtain high-resolution $PM_{2.5}$ we reran simulations for 3-yr periods around each nominal decade through 2070 to match the timespan of the energy decarbonization simulations that also extended through 2070. As impact metrics for PM are based on annual averages, which show little interannual variability, three year averages provide robust results. SSP simulations extend through 2100, and hence impacts related to temperature are sometimes assessed for the entire 21st century. For comparison, air pollution-related impacts over 2080-2100 are estimated based on extrapolation of the relatively slow rates of change seen in PM and ozone by the end of the air pollution simulations.

Impact Analyses: Mortality

We rely upon peer-reviewed studies performing epidemiological analyses of public health impacts of both climate and air pollution. In such studies, the health of hundreds of thousands or even millions of people are tracked over time, establishing a statistical relationship between exposure and health impact. This is similar to research relating cigarette smoking to health impacts.

As stated in the main text, our analysis of the impacts of ozone exposure on premature death is based upon the responses reported in one of the largest studies to date that uses the American Cancer Society Cancer Prevention Study-II (ACS CPS-II) cohort (Turner et al., 2016). This analysis calculated cause-specific deaths attributable to incremental changes in the maximum daily 8 h average O_3 concentration (MDA8) using a version of this cohort that spans 22 years of follow-up and included 669,046 subjects who experienced 237,201 deaths. Premature mortality attributable to long-term ozone exposure is calculated using well-established methods (e.g. Anenberg et al., 2010; Malley et al., 2017), as described in the equations below.

$$\Delta X = \begin{cases} 0 & if\ [O_3]\ \leq TMREL \\ [O_3] - TMREL & if\ [O_3]\ > TMREL \end{cases}$$

$$AF = 1 - exp^{-\beta \Delta X}$$

$$\Delta Mort = y_0 \times AF \times Population$$

where TMREL is the theoretical minimum risk exposure level (i.e. the 'counterfactual') in ppb, ΔX is the ozone exposure in a particular grid box above the TMREL, β is the coefficient of exposure-response relationship (i.e. the slope of the log-linear relationship between the change in exposure and mortality from the epidemiological study), AF is the attributable fraction of the disease burden related to long-term ozone exposure, y_0 is the cause-specific baseline mortality rate, population is the population count in a particular grid box of persons aged 30 years or older, and ΔMort is the estimated number of premature, cause-specific mortalities attributable to exposure to ozone levels above TMREL. Note that TMREL is set simply as the minimum ozone exposure reported in the epidemiological study, in this case 26.7 ppb. There is no compelling

evidence that exposure to levels lower than those at which data is available is safe, however. Hence this aspect of the method is a conservative one. To give an indication of the increased risk associated with ozone, the risk of respiratory-related premature fatality increases by 12±4% per additional 10 ppb ozone above TMREL and the risk of cardiovascular-related premature fatality increases by 3±2% per additional 10 ppb ozone above TMREL.

As noted in the main text, the analysis of the impacts of $PM_{2.5}$ exposure on premature death is based upon the results of a meta-analysis including 41 cohort studies from around the world, including the US (Burnett et al., 2018). Among other findings, that study concluded that the all-cause impact of $PM_{2.5}$ exposure was on the order of 30% greater than the sum of the response to the five previously established specific causes of death (ischemic heart disease (IHD), stroke, chronic obstructive pulmonary disease (COPD), lung cancer, and lower respiratory infections). It also reported worldwide impacts that were 120% larger than those based on the previous exposure-response function developed by the same group and widely used (e.g. in the Global Burden of Disease). Owing to the non-linear nature of the exposure-response function it is not possible to give a single value for increased risk associated with increased $PM_{2.5}$ exposure, but for the relative low exposures typically found in the US an indicative value is that risk of premature death due to non-communicable diseases plus lower respiratory infections increases by about 1% per $\mu g\ m^{-3}$ additional exposure. Additional discussion of how the results using this exposure-reponse function compares with other exposure-response functions is given below (see *Impact Analyses: Comparison of Present-day Health Results with Prior Studies* section). Deaths are evaluated for adults older than 25 based on the response to modeled exposures obtained with the Global Exposure Mortality Model (GEMM) described in the meta-analysis study. The low exposure threshold in this analysis is 2.4 $\mu g\ m^{-3}$, such a low value that unlike for ozone it has little impact on the results.

Exposure to heat can compromise the human body's ability to regulate its internal temperature, potentially leading to temperature-related deaths (Sarofim et al., 2016). Temperature and mortality are linked not only at hot extremes, such as during heatwaves, but also at temperatures that are moderately hot (e.g. Lee et al., 2014). The estimates presented here use the generalized risk function covering the US for hot temperatures above the local optimum temperature derived in a prior study (Shindell et al., 2020):

$$RR = 1 - 0.0014 \times (SMT - 30.9)T^2 + 0.005 \times (SMT - 26.7)T$$

where RR is relative risk, SMT is the local summer mean temperature (June–August) and T is the local daily temperature in °C above the optimum temperature where the latter is represented by each location's 84th percentile temperature (Honda et al., 2014). For US conditions, this relationship implies a stronger increase in RR at the highest temperatures in cooler locations, consistent with the underlying epidemiological data used to derive the generalized function (Weinberger et al., 2017; Shindell et al., 2020). This generalized risk function has been shown to capture the observed shape of the exposure-response curve in each of the 10 US cities that were used in prior evaluation of its performance (Shindell et al., 2020). As with other impacts, mortalities are estimated using:

$$\Delta Mort = y_0 \times AF \times Population$$

where the attributable fraction AF is defined as (RR-1)/1, y_0 is the all-cause baseline mortality rate and Population is the all-age local population. In evaluations of projected mortalities, the present-day value for the 84th percentile optimum temperature is used, but projected time temperatures are used for the summer mean temperatures, in order to represent adaptation to changing climatological background conditions (Shindell et al., 2020). In other words, we assume that people living in cooler climates develop shallower risk curves as they acclimatize to warmer summers via either physiological change, personal habits or changes to the built environment. In prior work, this has been shown to reduced estimated changes in heat-related premature deaths by ~40-45% relative to values without adaptation, and to provide similar estimates to adaptation based upon a lagged-response to the change in the temperature distribution (including extremes) rather than the change in summer mean temperatures (Shindell et al., 2020).

Changing risk due to exposure is combined with data on baseline public health and population distributions, along with projected changes in those factors, to evaluate overall health burdens on the US population. Population projections are from the socio-economic modeling associated with each individual SSP (Jones & O'Neill, 2016). These are applied at the country-level using the year 2015 distribution of population in the US (CIESIN, 2005) but also accounting for the slight increase from 85% to 94% for the urban share of population from 2020 to 2070 in the projections. The projected US population varies greatly across the scenarios, even as to the direction of change relative to the current (2020) population of about 340 million. Under SSP5, the US population swells to 581 million in 2070, whereas under SSP1 and SSP2 it rises more modestly to 440-450 million, under SSP4 it increases to 390 million and under SSP3 it decreases to 315 million. As our standard reference case is SSP3, this means that all climate policy cases (which use the other SSPs) have higher population, thereby reducing the health benefits when evaluated in terms of total numbers. Our analysis therefore examines per capita impacts as well as total health burdens since the latter are quite sensitive to these population projections. In particular, the benefits of the lowest warming scenarios which are under SSP1 are realized by a population 43% larger than that projected under the reference case SSP3 in 2070, greatly reducing their apparent value when viewed in terms of total burdens. These population projections are applied for both mortality and morbidity calculations.

The projections of future baseline mortality including cardiopulmonary disease, respiratory disease and malignant neoplasms are from the International Futures (IF, Hughes et al., 2011) model version 7.45 base scenario (http://pardee.du.edu/access-ifs, accessed September 23, 2019). This model projects cause- and country-specific baseline mortality rates through 2100, hence we have a single projection applied across all scenarios. More recent work applying the IF model to the SSPs supports the use of a single scenario for the US as it showed that for high-income countries the projections are extremely similar across the five pathways (Sellers, 2020). In this projection, baseline mortality rates in the US decline for all cause-specific deaths across all age groups except for slight increases in diabetes in younger persons (<40 years) and in respiratory deaths in the oldest population (>80 years). Deaths from cardiovascular diseases decrease most strongly, with, e.g., values in 2050 that are only 48-60% of those in 2015 across all age groups. For each underlying disease we calculate the baseline mortality rate changes between the future year (e.g. 2050) and 2015 and then we apply this relative change to the 2015 Global Burden of

Disease (GBD) baseline mortality (Stanaway et al., 2018). GBD baseline mortality rates were mapped to best match the current International Classification of Diseases (ICD) codes for respiratory (ICD-10 Codes: J00-J98; GBD Codes: B.3, A.2.3, A.2.4) and cardiovascular (ICD-10 Codes: I20-I25, I30-I51, I60-I69, I70; GBD Codes: B.2.2, B.2.3, B.2.8, B.2.9, B.2.10) related deaths for which significant impacts were found in the epidemiological study (Turner et al., 2016). For ozone-related impacts, the IF cardiovascular and respiratory changes were mapped to those impacts. In the case of impacts for which the epidemiology has provided links to broader mortality rates, we apply the nearest match from the IF data: all-cause except accidents is matched to non-communicable plus communicable diseases for heat exposure and non-communicable diseases plus lower respiratory infections is used for the all-cause impacts of $PM_{2.5}$ (consistent with the GEMM).

Uncertainties are based upon the combination of the 95% confidence interval associated with each of the exposure-response functions and the physical response uncertainty evaluated based upon the variation across ensemble members for future simulations. The former are geographically uniform whereas the latter are calculated at both the national and state level since variability is location dependent and the US states vary so greatly in size that the variability across simulations also varies markedly across states (it is roughly inversely proportional to their size). Values for exposure-response uncertainties are approximately ±33% for ozone (Turner et al., 2016); ±16% for PM (Burnett et al., 2018); ±35% for heat (Shindell et al., 2020).

Impact Analyses: Morbidity

As introduced in the main text, morbidity impacts of $PM_{2.5}$ are based on a systematic review and meta-analysis of literature describing responses for hospital admissions (HA), asthma-related emergency room visits (ERV), and childhood bronchitis cases described in detail elsewhere (Ru et al., 2020). Briefly, in the meta-analysis for HA, we separate impacts into those associated with cardiovascular disease and those related to respiratory disease. Cardiovascular diseases are defined as either codes 390–459 based on the International Classification of Diseases, Ninth Revision (ICD-9), or I00-I99 based on the Tenth Revision (ICD-10). For the latter revision, these include cardiovascular diseases (CVD-ICD I00-I99, except I88), arrhythmia (ICD10: I46-I49), cardiac diseases (ICD10: I00-I59, I97.1, I98.1), cardiac failure (ICD10: I50); ischemic heart disease (ICD10: I20, I21, I22, I24, I25.2), myocardial infarction (ICD10: I21, I22) and stroke (ICD10: I60-I66, I67 (except I67.0, I67.3), I68 (except I68.0), I69). Similarly, respiratory impacts are defined as hospital admissions classified with codes 460–519 in ICD-9 or codes J00-99 in ICD-10. For ICD-10, these include the broad category diseases of the respiratory system (J00-J99), which in turn encompass acute upper respiratory infections (J00-J06), pneumonia (J12-J18), chronic obstructive pulmonary disease (J41-J44), and asthma (J45-J46), among others. We did not include studies that only focused on specific causes within the above groups. In other words, we are reviewing the increased risk in “all-cause” cardiovascular and respiratory hospital admissions.

The exposure-response function (ERF) for the relationship between $PM_{2.5}$ exposure and cardiovascular HA is based upon 32 studies, with separate ERFs for population <65 and >65 years of age. Our ERF for the relationship between $PM_{2.5}$ exposure and respiratory HA is based

upon 41 studies, with a single all-age ERF as no significant differences were observed for different population subgroups. The ERF for asthma-related ERV is based upon 27 observations reported in 17 studies. Among those, 9 observations were focused on child asthma ERV, but statistical tests did not indicate a significant difference between the effects on children and those on adults. We thus constructed an ERF for the all-age population based on the pooled results of all the studies. Our meta-analysis for bronchitis included 3 studies documenting the relationship between acute symptom days of bronchitis and $PM_{2.5}$ exposures, all of which were focused on children (ages 1-19). The counterfactual level is found to be 5 $\mu g/m^3$.

For each morbidity endpoint, we constructed both log-linear and non-linear ERFs. The log-linear exposure-response model is described by:

$$HR = \exp(\beta x)$$

where HR is the hazard ratio, β is the coefficient of the exposure-response effect, and x is the exposure to $PM_{2.5}$. By definition, the logarithm of the HR increases at a constant rate β with increasing exposure. The non-linear ERF has two additional parameters, μ and τ, to allow curvature and location of the ERF to change across the range of exposure. This modeling approach was originally developed by Nasari et al. (2016) and was applied in Burnett et al. (2018). This ERF is expressed as:

$$HR = \exp(\theta \mathrm{T}(\mathrm{x}))$$

where

$$T(x) = \mathrm{f}(\mathrm{x})\omega(\mathrm{x})$$
$$f(x) = \mathrm{x}, \text{ or } f(x) = \log(\mathrm{x}+1)$$
$$\omega(\mathrm{x}) = 1/(1 + \exp\{-(\mathrm{x} - \mu)/(\tau \mathrm{r})\})$$

where θ is the regression coefficient, (μ, τ) are parameters, x is the exposure and r is the 5^{th}-95^{th} percentile range of exposures in the underlying studies. The two forms of $f(x)$ allow this ERF to behave as either a log model (when $f(x) = \log(\mathrm{x}+1)$, $HR = \exp(\theta \log(\mathrm{x}+1)\,\omega(\mathrm{x}))$ or as a log-linear model (when $f(x) = \mathrm{x}, HR = \exp(\theta\, \mathrm{x}\omega(\mathrm{x}))$. Note that when ω(x)=1 and $f(x) = \mathrm{x}$, this functional form becomes identical to the log-linear model above (i.e. $HR = \exp(\theta \mathrm{x})$). The function ω(x) is a logistic weighting function, where μ and τ control the shape. As such, the effect size becomes a non-linear function of x, instead of being constant across the range of x.

Finally, the HR calculated from the ERFs above is then used to derive AF:

$$AF = 1 - 1/HR$$

where AF is the fraction of total morbidity burdens at a specific location attributable to the $PM_{2.5}$ exposure, such that similar to mortality:

$$\Delta Morbidity = y_0 \times AF \times Population$$

where y_0 is the baseline morbidity rate of each endpoint, and population is the total population in the age groups applicable for a given morbidity endpoint. All results presented in this paper for future simulations use the log-linear model (the more conservative of the two). Note there are also morbidity impacts of heat, not included here, including on mental health-related emergency room visits (Basu et al., 2018).

An additional morbidity endpoint included in our analysis is the effect of $PM_{2.5}$ exposure on dementia. This estimate is based on the recent meta-analysis of Ru et al. (2021) that developed exposure-response functions based upon cohort and case-control epidemiologic studies reporting a quantitative measure of risk of dementia due to long term exposure to particulate matter. The

analysis encompassed all major types of dementia, including Alzheimer's disease, vascular dementia, and "other dementia", and was motivated by the growing recognition of the role of PM exposure in dementia onset. For example, the Lancet Commission report on Dementia identified air pollution as a dementia risk factor with "newer, convincing evidence" (Livingston et al., 2020). Though the analysis developed response functions for both dementia onset and premature death associated with dementia, to avoid any potential double-counting between dementia-related deaths and the 'all-cause' $PM_{2.5}$-related deaths in our mortality evaluation we only include dementia incidences in this study.

Impact Analyses: Comparison of Present-day Health Results with Prior Studies

To put our results into context with earlier studies, we examined the near present-day impacts on population health and compare with earlier publications of the same. Using our modeled surface ozone, we estimate 57,000 premature deaths due to ozone in the US in 2020. Using observations along with statistical infilling to represent missing areas, Seltzer et al. (2018) estimated 51,000 annual premature deaths for the US in 2015. Adjusting for the increase in population from 2015 to 2020 under the SSP1 scenario, the value derived from observations becomes 53,000, in close agreement with the results from our modeling. As was the case in the observation-based analysis of Seltzer et al. (2018), these results are roughly three times larger than those that would be obtained using the older ERF (Jerrett et al., 2009) that has a lower risk for respiratory disease and does not include cardiovascular disease. That older ERF is still widely used, for example by the US EPA in their Benefits Mapper, although both ERFs were derived from the work of the same researchers. Hence it is not surprising that our impacts are larger than those commonly reported. As in prior simulations with the GISS model, surface ozone tends to be overestimated in the US (Seltzer et al., 2017), and so we have adjusted the modeled ozone to remove this systematic bias as in prior studies (Shindell et al., 2018). The CMIP6 version of the GISS model has improved surface ozone relative to prior versions, so that the bias adjustment is smaller and is now applied as a constant multiplication by 0.86. Assuming a constant fractional bias produces smaller health impacts from declining ozone than assumption of a constant absolute bias, hence we adopt that as the more conservative bias correction.

Our modeled 2020 population-weighted $PM_{2.5}$ concentration across the contiguous US is 8.9 μg m^{-3} in the decarbonization simulations, and it is 7.0 μg m^{-3} in the SSP runs (in each case reporting the 2016-2025 average). For comparison, the comparable population-weighted concentration calculated from the widely-used dataset produced by using satellite observations of aerosol to adjust a global model's simulated $PM_{2.5}$ concentration is 9.3 μg m^{-3} for 2014-2016, the latest years available (Shaddick et al., 2018), and the value estimated by US EPA scientists using a data fusion of surface monitoring and a high resolution regional model was 8.4 μg m^{-3} for 2014 (the most recent year analyzed; Fann et al., 2018). The differences between our two sets of simulations stem from the higher $PM_{2.5}$ precursor emissions in the decarbonization runs (from IIASA) relative to those in the SSPs (from CEDS) for NO_x (3.7 vs 2.8 Tg yr^{-1}; see Figure 1), BC (0.27 vs 0.17 Tg yr^{-1}), and the inclusion of additional 0.8 Tg yr^{-1} $PM_{2.5}$ in the IIASA inventory that is not associated with specific species (e.g. fly ash). The decarbonization simulations therefore produce a larger amount of $PM_{2.5}$ than the SSP simulations. The R^2 correlation between our modeled 2020 field from the decarbonization simulations and the satellite/model field over

all 0.5 x 0.5 degree boxes is 0.69, consistent with prior findings that the use of higher-resolution PM fields from the model by employing within grid box emissions gradients during simulations leads to more realistic simulated PM in urban areas (Shindell et al., 2018). Examining the average value without population weighting (though all values are area-weighted), the value in the decarbonization runs is 5.1 μg m^{-3} for 2020, whereas the value estimated by US EPA scientists was 5.2 μg m^{-3} for 2014 (Fann et al., 2018), again showing good agreement. Given the agreement between our decarbonization simulations and other analyses informed by surface and satellite observations, we do not perform any bias adjustment on those simulations. As was done for ozone, we do bias-adjust the SSP simulated $PM_{2.5}$, however, including a uniform scaling of 1.25 (except for the NYC area, where the scaling is instead 0.825 to account for an apparent local overestimate there).

Turning to $PM_{2.5}$-related mortalities, our 2020 value is 191,000 annual premature deaths in the US using the latest exposure-response function based on an expanded dataset (Burnett et al., 2018). In comparison, US EPA researchers estimated that exposure to particulate matter caused 121,000 premature deaths in 2014 in the United States (Fann et al., 2018) in an analysis using the older exposure-response function from the same team of researchers (Burnett et al., 2014). Our larger values are consistent with the greater responses reported in the meta-analysis of epidemiological studies that showed ~120% larger values relative to the older risk function (Burnett et al., 2018). In fact, using satellite-informed modeled surface $PM_{2.5}$ concentrations, Burnett et al. (2018) report 213,000 premature annual deaths from $PM_{2.5}$ in the USA and Canada for 2015, a value slightly larger than our results which seems to correspond well to the inclusion of Canada and the slightly earlier year for their analysis. An analysis based on another recent meta-analysis (Vodonos et al., 2018) finds even higher $PM_{2.5}$-related deaths in the US than using the 2018 Burnett et al function (Vohra et al., 2021), suggesting that if anything our large impacts may nonetheless be conservative.

Evaluating the premature deaths attributable to heat exposure in the US, we find ~17,000 for 2020 (based on the 2016-2024 average). Our prior analysis found 12,000 (7,400-16,500 for the 95% CI) premature deaths attributable to heat exposure for 2010 (Shindell et al., 2020). Accounting for the population increase from 2010 to 2020 would increase that value from 12,000 to 13,500, suggesting that the bulk of the increase is due to the rise in temperatures which have jumped roughly 0.3ºC in the US over this last decade (NASA GISS; https://data.giss.nasa.gov/gistemp/graphs_v4/). Most other prior analyses examined only a subset of US cities, and hence found substantially smaller impacts.

Several prior studies have looked at some of the morbidity impacts considered here. The most relevant is a US EPA analysis of 2014 health burdens in the US (Fann et al., 2018). That study included cardiovascular and respiratory HA, asthma ERV, child bronchitis and work lost days due to PM-exposure. In each of those cases, their values are generally fairly similar to those in our analysis, though typically closer to our log-linear results than to the values using our non-linear exposure-response functions (Table S2). The exception is our acute child bronchitis, for which our log-linear value is much lower. Our value without a counterfactual, however, is 186,000, much closer to the reported EPA value that did not use a counterfactual (for other endpoints the effect of a counterfactual is much smaller, less than 5%, as observations extend to lower levels). Since, as noted earlier, we had similar PM exposures as in the EPA analysis,

differences between our values are dominated by our updates to exposure-response functions and the use of a counterfactual for child bronchitis. There are also some methodological differences, such as the EPA's use of 10-yr age bins for HA and asthma ERV whereas we have two groups (<65 and >65) for cardiovascular HA and just one for respiratory and asthma ERV as our meta-analysis indicated this was better supported by the available data. For work lost days due to heat, our results are substantially smaller than those reported by Watts et al (2020). The sources of this discrepancy are not clear. Their study used a method designed to be globally applicable, whereas our analysis is based on empirical data for the US and hence may be more appropriate for a national analysis. Their method also incorporated relative humidity whereas ours is based solely on temperature, which may again be responsible for at least some of the differences. As our values are much lower than the others, we suggest that our results can be viewed as quite conservative.

Table S2. Comparison of 2020 Morbidity results with prior studies

Impact	Prior studies	Our values for 2020
Cardiovascular HA	29,000[a]	40,000 (ll); 105,000 (nl)
Respiratory HA	27,000[a]	35,000 (ll); 132,000 (nl)
All-age Asthma ERV	68,000[a]	47,000 (ll); 106,000 (nl)
Child Asthma Hospitalizations	na	4,400 (ll); 11,000 (nl)
Adult Asthma Hospitalizations	na	1,100 (ll); 6,900 (nl)
Acute Child Bronchitis	160,000[a]	85,000 (ll); 324,000 (nl)
Work Lost Days due to PM	16,000,000[a]	13,000,000
Work Lost Days due to heat	250,000,000[b]	51,000,000

Prior studies: a – 2014 values from Fann et al., 2018; b – 2019 value from Watts et al., 2020.
Our values: names refer to the exposure-response function, where ll is log-linear, nl is non-linear.

Impact Analyses: Labor Productivity

We evaluated the effects of both air pollution and heat exposure on labor productivity. Labor losses due to exposure to extreme heat are evaluated using previously established exposure-response functions for the US (Graff Zivin and Neidell, 2014), as described in detail in Zhang and Shindell (2021). In brief, nationally representative survey data from 2003 to 2006 and daily weather observations from roughly 8,000 weather stations were used to investigate how Americans allocate their work and leisure time as a function of ambient temperatures. A statistically significant approximately linear decrease in the time allocated to labor with increasing temperatures was found for high-risk sectors when value exceeded a threshold of about 29°C. This relationship has been used in several recent studies (Hsiang et al., 2017; USGCRP, 2018). In our calculations, the value of time lost is calculated using county-level annual employment (covering working ages 15-64 years old) and annual average weekly wages from the Quarterly Census of Employment and Wages, U.S. Bureau of Labor Statistics. We use the North American Industry Classification System (NAICS) to determine the number of workers in high-risk industries/sectors (largely those that cannot readily be air-conditioned):

NAICS 11 for agriculture, forestry, fishing and hunting; NAICS 23 for construction; NAICS 31-33 for manufacturing; NAICS 21 for mining; NAICS 48-49 for transportation, and NAICS 22 for utilities (https://data.bls.gov/cew/doc/titles/industry/industry_titles.htm, accessed Jan 10, 2019). The 2016 fraction of workers in high-risk industries is used for each county and is held fixed through time. Within the SSPs there are substantial changes projected in the age distribution and education level of the population (KC and Lutz, 2017). Although both of these factors will play a role in determining the future workforce, and these have been used to indirectly infer possible changes in the total workforce in the future, they do not reveal the distribution of workers within different occupations. In particular, the growth in the labor force can differ significantly from the growth in the working-age population for younger age groups with longer time spent on education or when taking into account rising labor participation rates for women (Foure et al., 2020). As our results are highly specific to those sectors at high-risk of heat exposure, we have not attempted to infer the impact of future workforce changes on the interaction between labor and heat or labor and air pollution but note that this is an area worth additional study.

The analysis covers the contiguous US. Surface temperature changes are based upon the daily temperature values modeled in the simulations, with results reported averaging lost hours over at minimum 10 years to reduce the noise inherent in daily temperature values (averages over more years are used for ensemble simulations SSP2_45, Current Path, Decarb Energy Global and Decarb Energy US). We note that in our prior work, we found that use of alternative exposure-response functions could lead to substantially different results in terms of total magnitude although spatial patterns were quite similar to those using the method employed here (Zhang and Shindell, 2021). The alternate exposure-response functions included daily relative humidity data, which was not saved from the simulations analyzed in this study. As the other exposure-response function yielded much larger (roughly double) the US impacts in the late 20th century, we emphasize that the results reported here are likely at the low end of impact potentials.

The effects of exposure to $PM_{2.5}$ on labor are evaluated based on a study relating such exposure to work loss days in the US for 1976-1981 (Ostro, 1987). As in similar analyses performed by the US EPA (2015), we calculate the HR as the average across years weighted by the variance of β each year, finding a mean of 1.047 per 10 $\mu g\ m^{-3}$ and a 5%-95% confidence interval of 1.04 to 1.05. These apply to the working age population, again defined as persons aged 15-64. Uncertainties for all morbidity outcomes are evaluated in a similar manner to those for mortality. Values for exposure-response uncertainties are approximately ±55% for the effects of temperature on labor based on the 95% CI (1.96 sigma) of the covariance between labor and maximum temperature (Graff Zivin and Neidell, 2014). Values for the impacts of air pollution on labor are ±20% (Ru et al., 2020; Ostro, 1987).

Impact Analyses: Agriculture

We also calculated the impacts of air pollution and climate change on agriculture. We evaluate wheat, maize (corn), soy and rice impacts using an empirical crop model based on statistical relationships for the impacts of temperature, precipitation, CO_2 concentrations, and ozone (rather than plant level simulations) (Shindell et al., 2019). Wheat, rice and maize responses to changes in meteorological variables are based on a meta-analysis of more than 1,000 modeling studies

(Challinor et al., 2014), incorporating relationships observed in field studies. Responses for soy to temperature are based upon a separate study (Zhao et al., 2017) as those were not included in the meta-analysis. We include separate temperature response coefficients for wheat, maize (corn), and rice according to temperate or tropical conditions. For ozone, we use the M7 and M12 exposure metrics (the mean 7- or 12-hr exposure during the growing season, depending on the crop). These affect yields based on the response reported in field studies (Wang and Mauzerall, 2004), and have been used previously for global crop modeling (Van Dingenen et al., 2009). The growing season is locally defined based on Van Dingenen et al. (2009).

Changes in temperature, precipitation and ozone in response to methane emissions changes are taken from the simulations performed for this study. In addition, CO_2 changes over time are accounted for. CO_2 fertilizes crop growth, especially for C3 plants such as wheat, soybeans and rice with only very small effects for maize (a C4 plant). These effects are included here based on relationships described previously (Tebaldi & Lobell, 2018). Crop distributions for 2010 are taken from the Food and Agricultural Organization data sets (faostat.fao.org) and are maintained at those levels in all calculations of impacts (i.e. no projected changes in crop areas are included). Uncertainties in the exposure-response for climate-related conditions (temperature, precipitation and CO_2 concentrations) are based upon Challinor et al. (2014) and for ozone are from van Dingenen et al (2009), with a total relative value of ~30% for the impacts evaluated here. Adaptation such as changing cultivars or changes in management practices are not included in these analyses.

Impact Analyses: Valuation

We evaluate both market and non-market costs associated with the impacts described above. All values are in constant 2018 US$ (adjusting from other years when necessary). Non-market values include those associated with premature death and many of the effects of climate change. Market costs include direct spending on health care and the effects of environmental changes on labor productivity.

Monetized benefits associated with avoided mortality are evaluated using a willingness-to-pay (WTP) measure of the value societies place upon reduced risk of premature death. This measure is often referred to as the value of a statistical life (VSL) though it is in fact an expression of the value that people affix to small changes in mortality risks in monetary terms rather than the value of any individual's life. Such valuations can be derived from empirical data, for example on the increased wages offered for occupations with a higher risk of death or expenditures on transportation safety measures. Health literature often uses disability adjusted life years, which are arguably more informative since they incorporate the age of the affected individuals, but for monetization VSL is a better-established metric in the economics literature (e.g Viscusi and Aldy, 2003). We base our WTP on the mean of 26 peer-reviewed studies evaluated by the United States Environmental Protection Agency (USEPA, 1997) and used by that agency to derive its official recommended VSL of $7.4 million in 2006$. That value is then inflated to represent the year 2018 using an economic growth rate of 3% yr^{-1} that leads to a value of $10.6 million.

For comparison, valuation of climate-related damages is also computed using a widely-used damage function developed for social cost of carbon estimates (Nordhaus, 2008). This function has damages proportional to the square of the temperature change and equal to 1.8% of world output at 2.5°C. A more recent analysis combining multiple climate impacts for the US also found a quadratic dependence on temperature and a similar, though slightly larger, sensitivity (Hsiang et al., 2017). We use GDP projections with time from SSP1 across all scenarios to facilitate comparison across scenarios as the SSPs envision very different trends of GDP that otherwise overwhelm the impact of climate (e.g. the 2100 GDP in SSP5 is ~4x that in SSP3). The average GDP growth rate in SSP1 is 'middle-of-the-road' with a value of 2.2% yr^{-1}. The portion of climate damages attributed to the US is based on the US economy's share of global GDP over time. For consistency, in the mortality valuation VSL increases along with per capita growth in GDP, since it's associated with the willingness-to-pay, also using the projections of SSP1 in all analyses.

For morbidity, the value of avoided hospital admission is based on the Healthcare Cost and Utilization Project, a US government-run health data project with a comprehensive dataset for inpatients (HCUPnet, 2020). Values range from $11,900 per visit for respiratory illness to $16,400 per visit for cardiovascular disease in persons over 65 and to $18,900 per visit for cardiovascular disease in persons under 65 years of age. Valuation of avoided asthma ERVs is based on Chastek et al. (2016) and is $91 per visit. Valuation of work loss days due to air pollution and of childhood bronchitis is based on the Carbon Reduction Benefits on Health (CaRBonH) calculation tool (Spadaro et al., 2018) adjusted for US conditions and are $216 per day and $1057 per case, respectively. Work losses due to air pollution are assumed to affect all sectors of the economy. Dementia valuation is based upon the findings of a systematic review of 42 cost-of-illness studies (Wimo et al., 2017). We utilize average values for the World Health Organization region containing the US and include the direct cost in social care and direct medical expenses along with indirect informal care costs from time spent assisting with daily activities and time spent in supervision of behavioral symptoms. Values are adjusted to 2018 USD.

To estimate the value associated with labor losses from heat, which do not affect all sectors, we use 2016 county-level annual employment (working ages 15-64 years old) and annual average weekly wages from the Quarterly Census of Employment and Wages, U.S. Bureau of Labor Statistics (www.bls.gov/cew/datatoc.htm, accessed Jan 10, 2019). National average wages range from $19.0 $hour^{-1}$ for agriculture to $44.9 $hour^{-1}$ for utilities and are spatially heterogeneous across the US.

For changes in crop production, valuation is based upon yield changes multiplied by the 2018 global market prices per tonne from the USDA and World Bank (indexmundi.com/commodities; which gives $164 for maize, $210 for wheat, $421 for rice and $394 for soybeans). This provides a fairly simplistic measure of the value of yield changes, as it clearly does not account for benefits such as those to subsistence farmers or to national food security.

2. Additional Analyses

GISS results in context with other CMIP6 models

In the main text, GISS model projections for US average annual average surface air temperatures were shown across scenarios and the projections under the SSP2_45 scenario were put in context with all available CMIP6 models. Analogous results are presented here for the global mean (Figure S9). As with the US, global mean values generally follow the intended radiative forcing in the SSP simulations. In the energy sector simulations, global decarbonization of the energy sector shaves off 0.5 ± 0.1°C of 1.6 ± 0.1°C additional warming projected for the 2061-2070 period relative to 2011-2030. Depending on emissions from other sectors, this level of decarbonization is therefore potentially consistent with a 1.5-2°C stabilization, as it is designed to be given that this scenario uses this sector's emissions under a 1.9 W m^{-2} scenario. Uncertainties (95% CI) at the global scale are fairly small, ~0.2°C, for decadal means from the GISS model. We note that the lack of clear near-term impacts on surface temperatures is a function both of the long response times of the climate system and the tendency for a shift away from fossil fuels to lead to reduced aerosol masking in the near-term that approximately balances the slow response of CO_2 (Shindell and Smith, 2019). Similarly, the low Near-Term Climate Forcer SSP3_70 scenario is similar to the baseline SSP3_70 scenario through at least 2040 (Figure S9) in part because the NTCF reductions include offsetting decreases in warming and cooling agents.

It is also worth noting that for context, we use the full CMIP6 ensemble (as available in Dec. 2020) but recognize that the spread in this ensemble of ECS and TCR exceed the constrained bounds of these values from observational data (e.g. Sherwood et al, 2020; Njisse et al 2020). However, the mean of the current CMIP6 models is only slightly higher than in CMIP5, implying only a small effect in the implications for this study. For surface pollutants, we use only the CMIP6 models with interactive composition, a smaller subset of the entire ensemble.

We examined summer (June-August) temperatures in CMIP6 models as a proxy for heat exposure leading to impacts on health and labor productivity. Figure S8 shows avoided June-August warming in the US under the 1.5°C scenario (SSP1_19) relative to the lower reference (SSP3_70) in the GISS model used in this study, in two other representative CMIP6 models, a near-median model (CNRM-ESM2) and a high-end model (UKESM1), and the mean across all CMIP6 models. At the national level, the 11 other CMIP6 models project June-August average avoided warming in SSP1_19 relative to SSP3_70 over the contiguous US from 1.1°C to 2.8°C, with a mean of 2.0°C. The GISS model has among the smallest values at 1.3°C, but shows larger differences in the western US and smaller differences in the eastern US than the CMIP6 mean, and in particular small values in and just east of the Ohio River Valley (Figure S8). Humans are sensitive to heat extremes, however, and so changes in summer means are not necessarily proportional to impacts.

To probe this further, we selected the same two illustrative models, one near the multi-model mean, CNRM-ESM2 with a US summer mean avoided warming of 1.8°C, and a high-end model, UKESM1-0-LL with a value of 2.6°C, and evaluated the impacts of their simulations' daily temperatures on heat-related mortality. These models were selected not only for their differences

across these scenarios, but also to capture the total projected change relative to the present. The UKESM model reported the largest warming under both scenarios, with the CNRM model in both cases reporting values near the mean. In contrast, the GISS simulations were near the mean under SSP3_70 but were among the warmest in SSP1_19, leading to the smaller avoided warming. The national totals in these other models were 12,000 yr^{-1} and 35,000 yr^{-1} based on CNRM and UKESM, respectively, bracketing the GISS value of 23,000 yr^{-1}. The lower value based on CNRM simulations suggests that changes in the temperature distribution play as important a role as changes in the mean. At the state level, variations are large across these three models in many parts of the country, especially the Northeast and Pacific Northwest. Though the values derived here are ~50% higher or lower than those using our model, this likely represents an upper limit to uncertainties as the UKESM model is an extreme case and the models have not been bias adjusted to correct for differences in baseline US temperatures (the US average present-day temperature ranges from <10° to >15°C across the CMIP6 models). The need for bias adjustment as well as the requirement for high temporal resolution data make multi-model intercomparisons particularly challenging for temperature and ozone-related impacts.

As noted in the main text, the evidence for a threshold for the onset of heat effects on labor (Graff Zivin and Neidell, 2014) makes those impacts highly sensitive to uncertainties in temperature projections. Using the same exemplar CMIP6 models as for heat/mortality, we find that 2070 lost labor hours due to heat exposure under the SSP3_70 reference case are more than twice as large based on UKESM than using CNRM or GISS. As such, the avoided impacts from climate change mitigation are quite model-dependent, with impacts 7 times larger using UKESM climate projections than in our analysis. Given our 'middle-of-the-road' warming under SSP3_70 along with relatively high warming under SSP1_19, the labor benefits from reduced heat-exposure seen in our analysis are likely to be conservative, perhaps markedly so. This is especially so given that we have a used an exposure-response function based on dry heat only that yields substantially smaller impacts than an alternative function based on heat and relative humidity (Zhang and Shindell, 2021). Hence further study of the probability distribution of temperature changes, the impact of bias-adjustment and the sensitivity to the exposure-response function utilized would be useful. Given the large uncertainties in labor response to heat exposure changes, these impacts are excluded from our web-based results.

For surface $PM_{2.5}$, we again compare projections in the GISS model with that in other CMIP6 models (Figure S10). Few models provide data for the SSP1_19 simulations. We therefore examine $PM_{2.5}$ from six models for the SSP1_26 and SSP3_70 scenarios using values constructed from aerosol fields using assumed size distributions as in Turnock et al. (2020). Note that these PM fields differ in several ways from those used in this analysis for the GISS model: they do not include nitrate aerosols, as those were not reported for most models, whereas we do include nitrate; they assume that $1/10^{th}$ of all dust is fine particulate whereas we use the fine fraction explicitly calculated in the GISS simulations; they use the native resolution aerosol fields whereas we use the higher-resolution fields calculated using tracer moments. In total, these lead to substantially smaller population-weighted $PM_{2.5}$ exposure, but they have the virtue of being consistent across CMIP6 models. All models show a substantial decrease in $PM_{2.5}$ levels averaged over sub-Arctic North America under SSP1_26 relative to SSP3_70, with the GISS model results similar to those of four other models. For example, the GISS model shows a decrease over North America of 0.40 μg m^{-3} in 2070 under SSP1_26 relative to SSP3_70, near

the 0.46 μg m^{-3} mean of the CMIP6 models. One model shows far larger decreases in $PM_{2.5}$ levels, which results from that model projecting a large increase in $PM_{2.5}$ under the reference case. Though markedly different than others in the difference between scenarios, two other models also project increases under SSP3_70, albeit much smaller ones.

For surface ozone, again few models provide data for the SSP1_19 simulations, and hence we compared surface ozone changes projected under the 2°C scenario (SSP1_26) relative to the lower reference (SSP3_70) in the CMIP6 models and in the GISS model used in this study (Figure S11). As with $PM_{2.5}$, all models show a substantial decrease over North America under SSP1_26 relative to SSP3_70. In this case, the GISS model results are at the high end of the small set of available results. For 2070, the GISS model shows a projected decrease in North American average values of 10.4 ppb versus a multi-model mean of 9.1 ppb. That value is 14% greater than the multi-model mean, with a range across other models from 5% larger to 33% smaller changes. We note that unlike with $PM_{2.5}$, for which the annual average exposure is the input to exposure-response calculations, ozone-related impacts are proportional to 8-hr daily maximum exposures (health) or seasonal exposures (crops) and so this analysis gives only a rough idea of how the impacts would vary across these models. Additionally, ozone rapidly falls below impact thresholds under aggressive climate change mitigation scenarios, however, so that ozone-related health impacts are not as sensitive to the uncertainty in ozone projections in those cases.

We also compared the spatial pattern of simulated surface ozone changes in the GISS model with those in other CMIP6 models (Figure S12). The comparison shows that the GISS results exhibit larger ozone declines than other models in the Northeast and Mid-Atlantic coast, with slightly smaller values in parts of the central Plains and Mountain West. A prior study reported that the GISS model used here showed the largest decrease under the SSP3_70 through 2050, during which time several showed increases under that scenario (Turnock et al., 2020; see their Figure S19), as also seen in our analysis (Figure S11). Note that analyses with simpler models also show decreases in surface ozone under the reference scenario (for the OECD; Rao et al., 2017), as in our model. The increases in reference case ozone in some models suggests that although our model shows larger reductions in ozone under SSP1_26 relative to SSP3_70 than others, the health impacts based on other model's ozone projections could be smaller or larger, as with larger values under SSP1_26 they would be less prone to falling below impact thresholds that lead to saturation in our impact analyses (as described in the main text and shown in Figure 3). Full impact analyses using data from other CMIP6 models would require hourly ozone to construct health and crop metrics, which is not available from many models and is beyond the scope of this study.

Additional results

The main text emphasizes mortalities, including providing cumulative totals over the next 50 years of 5.8 million avoided premature deaths summed over all causes for our illustrative example comparing the 1.5°C scenario relative to the reference (SSP3_70) scenario. Those cumulative totals are made up of 2.3 million for ozone-related, 3.4 million for $PM_{2.5}$-related, and 150,000 for heat-related avoided premature deaths, respectively.

Morbidity impacts related to $PM_{2.5}$ exposure generally follow the temporal development of $PM_{2.5}$-related mortality. Figure S2 shows several examples of non-fatal impacts of air pollution on health and labor. The child and adult asthma hospitalizations given in the main text are a subset of the total respiratory hospital admissions shown here.

Figures S3 and S4 show avoided crop yield losses under the 1.5°C scenario (SSP1_19) relative to the lower reference (SSP3_70) for maize, rice, soy and wheat. As noted in the main text, the ozone decreases under the 1.5°C scenario are always beneficial to crop productivity. These occur mostly during the first decade as precursor emissions decrease and change more slowly thereafter as precursor emissions decrease modestly after 2030 under both 1.5°C and reference scenarios (Figure S1). Climate change leads to initial yield decreases (increased losses) due to reduced CO_2 fertilization (though increased CO_2 may lead to reduced nutritional value (Meyers et al., 2014)). The impact of climate change mitigation switches sign over time, as warming in the mitigation scenario departs significantly from the stronger warming in the reference scenario and has a larger impact than CO_2. The reduced yield losses due to avoided warming augment the ozone-driven yield increases, reaching comparable or larger magnitudes by 2070. The spatial patterns of total impacts are highly inhomogeneous, primarily reflecting the spatial pattern of cultivation of these crops (Figures S3 and S4). The 2070 losses of ~1,200 kt wheat, ~3,000 kt maize, ~100 kt rice and ~3,000 kt soy correspond to about 3, 1, 1 and 5% for these crops, respectively. These relative yield losses are evaluated based on 2010 US production from the FAO, which is 38,246 kt wheat, 220,650 kt maize, 7,605 kt rice and 59,299 kt soy. Future production levels might be higher or lower, however. As noted in the main text, the cumulative benefits for the US over the next 50 years of a 2°C pathway relative to the lower reference SSP3_70 are ~440 million tons of avoided yield losses. Comparing the more ambitious 1.5°C pathway with that same reference increases the benefits to 530 million tons.

The near-term net climate-related impacts of ambitious policies (1.5°C relative to SSP3_70) are damaging for agriculture, which does not occur for health or labor impacts. The fact that CO_2 affects yields makes the separation into 'air pollution' and 'climate' pathways ambiguous, however, underscoring the logic of examining impacts regardless of physical pathway. Furthermore, as noted in the main text, including both air quality and climate changes the impacts of ambitious policies are always beneficial for agriculture (Figures S3 and S4).

Figures S5, S6 and S7 show the valuation of labor impacts and morbidity impacts over time. For context, the valuation of non-fatal impacts is small compared with the valuation of the reduced risk of premature death. For example, comparing the 1.5°C scenario (SSP1_19) relative to the reference (SSP3_70) and with a 2.5% discount rate, the monetized benefits related to reduced risk of premature death are $980 billion in 2070 whereas they are $3.2 billion for avoided labor losses, $1.9 billion for avoided costs associated with dementia, $1.4 billion for avoided crop losses, and $110 million for avoided hospitalizations and ER visits. Analogous cumulative values are $54 trillion for reduced risk of premature death, $111 billion for avoided dementia costs, $53 billion for avoided labor losses, $72 billion for avoided crop losses, and $10 billion for avoided hospitalizations and ER visits. As in prior analysis, the morbidity cost of dementia including both direct and indirect care costs is particularly large relative to other air pollution-related morbidity impacts, but still small in comparison with the mortality valuation.

Valuation of air quality-related health benefits under 1.5°C or 2°C scenarios in a prior study finds ~$2-3 trillion in benefits in the US for 2020-2050 with 3% discounting (Markandya et al., 2018). We have roughly 10 times larger impacts (Figure 7), with several factors responsible for the differences: we use updated epidemiology with larger risk increases per unit air pollution exposure, we include additional impacts of both ozone and $PM_{2.5}$ exposure, we compare with a higher reference case (SSP3_70) whereas their reference is SSP2 (~6.5 W/m^2 target forcing), we use the US EPA's value of a statistical life rather than the much lower OECD value used in the other study, and their analysis is based on the GCAM IAM and the FASST screening model whereas ours is based on emissions projections from different IAMs and a full composition-climate model (which, e.g., includes the effects of climate change on air pollution).

Since we only quantified effects of heat-exposure in our analysis, we also utilized a broader measure of climate change to characterize climate damages along the scenarios. We then compared the valuation associated with the health impacts of heat exposure with those broader climate damages. For the latter, we estimate overall climate-related damages (including heat exposure) as used in social cost of carbon calculations (see Methods). Such estimates attempt to include valuation of increases in damages from factors such as extreme events and sea-level rise in addition to direct effects on human health. We find that our values for the fatal effects of heat exposure alone are larger than the total climate-related damage estimates for aggressive mitigation relative to the high SSP5_85 reference (Figure 7). This suggests that our valuation of heat-related premature mortalities is not necessarily greatly underestimating total climate-related impacts, as those may be heavily weighted by the large value society assigns to reduced risk of human deaths, and that in fact typical estimates of climate-related damages may be substantially too low, as in other recent analyses (Carleton et al., 2019). Standard climate-related damage estimates are larger than our values for the fatal effects of heat exposure in comparison with the lower SSP3_70 reference case, however, indicating that the ratio of these damage estimates is highly scenario-dependent. In either case, our values for heat-related deaths will of course be lower than the total impact of climate damages. Even the full change in climate-related damages in response to mitigation policies would be smaller than the air pollution-related damages over the next several decades, however, indicating that analyses of the benefits of decarbonization using the social costs of carbon are likely missing the bulk of the societal benefits.

Correlations between mortality impacts and emissions

Our analysis of a large number of scenarios allows us to explore relationships between emissions and impacts. For premature deaths, we find that air pollution-related deaths are roughly proportional to regional NO_x emissions whereas heat-related deaths are roughly proportional to global CO_2 concentrations. Across all scenarios (Table S1), the R^2 correlations between decadal impacts and emissions are 0.82-0.84 for ozone-related or $PM_{2.5}$-related deaths and US NO_x emissions, and for heat-related deaths and global CO_2 concentrations (Table S3). In contrast, they are <0.12 for air pollution-related deaths and global CO_2 concentrations or for heat-related deaths and US NO_x emissions. Note that high correlations can be found for the latter cases under single scenarios since they vary consistently with time, but the cross-scenario analysis suggests there is causality in those cases. NO_x emissions serve as a proxy for all air pollutants in this

analysis as does CO_2 for all greenhouse gases, but both appear to work well. Excluding the SSP3_70Low scenario leads to higher correlations between air pollutant-related mortalities and global CO_2 concentrations, but the values are still quite low (0.11 for PM and 0.21 for ozone). Correlating instead with CO_2 emissions, values rise to 0.61 for PM and 0.68 for ozone across all scenarios, but heat-related deaths lose their high correlation dropping to 0.09. In this case, excluding the SSP3_70Low scenario leads to correlations roughly equivalent to those seen for NO_x, with values of 0.81 for PM and 0.91 for ozone. Hence in many cases, it appears that CO_2 emissions would provide a good proxy for air pollution-related deaths, though they do not work well in a case in which climate change mitigation is not the main priority nor do they work well for heat-related deaths.

Table S3. Correlations between Drivers and Responses

Mortality from exposure to:	Correlation with US NO_x emissions	Correlation with global CO_2 concentrations	Correlation with global CO_2 emissions
Ozone	0.82	0.11	0.68
PM	0.84	0.05	0.61
Heat	0.05	0.82	0.09

Correlations are R^2 values across the decadal results from all scenarios of Table S1.

Additional discussion of valuation

Several additional values for benefit valuation based on the data shown in Figure 7 are presented here to facilitate comparison with other publications. Over the 2020-2050 period, damages are $4 trillion due to heat (SSP1_26 vs SSP5_85) and $64 trillion due to air pollution (no discounting) and for 1.5°C they are $6 trillion and $81 trillion, respectively. Using the SCC the avoided damages over this period are $3 trillion (SSP1_19 vs SSP5_85, no discounting). Over this same time period but comparing with the lower reference case, our benefit values for 2°C and 1.5°C relative to SSP3_70 are $24 and $34 trillion, respectively.

These are much larger than the estimated policy costs of $8.4 and $9.9 trillion over this period for the entire economy (Markandya et al., 2018), or based on analysis of additional spending in the energy sector alone, values of ~$3.3 trillion (McCollum et al., 2018) or ~$2 trillion in a very recent update (Williams et al., 2021). In computing the benefit/cost ratios shown in Figure 7 we utilized the time dependence of Williams et al for all three analyses as the other two cost analyses reported only totals over the period through mid-century. As costs were fairly level between 2040 and 2050 in Williams et al., we extrapolated that same spending to 2060 as well to extend the analysis slightly in Figure 7 so that the transition to the benefit/cost ratio passing 1 that is discussed in the main text could be seen for the Heat/Markandya case. We note that mitigation costs from McCollum et al. (2018) and Williams et al. (2021) might be considered inherently low as they include only the energy sector. Costs in other sectors can be small or sometimes be difficult to determine, however, as they involve lifestyle and behavioral choices. For example, reducing food waste or changing diets to reduce agricultural emissions or halting deforestation are all actions that are not readily monetized. We therefore include all three

mitigation cost estimates for the US in our analysis, though we acknowledge that comparison between SSP1's low warming scenarios and reference cases from SSP3 and SSP5 include many differences in underlying socio-economic developments that form part of the transition to the sustainable world envisioned under SSP1.

For 2050 and 2100, we find that the 2050 benefits are ~$5-6 trillion per year and the 2100 benefits are ~$14-15 trillion per year including both air pollution and climate (SSP1_26 vs SSP5_85). The IPCC Special Report on 1.5°C (Hoegh-Guldberg et al., 2018) reported that for the US, holding warming to 2°C leads to a reduction in economic damages associated with climate change of ~3.5% of GDP in 2100 (based on Yohe, 2017 and Hsiang et al., 2017). This translates to about ~$2 trillion per year. Yohe (2017) reported a value for 2°C relative to no-policy of ~0.7% of GDP for 2050, which translates to about ~$250 billion per year (range ~140-350).

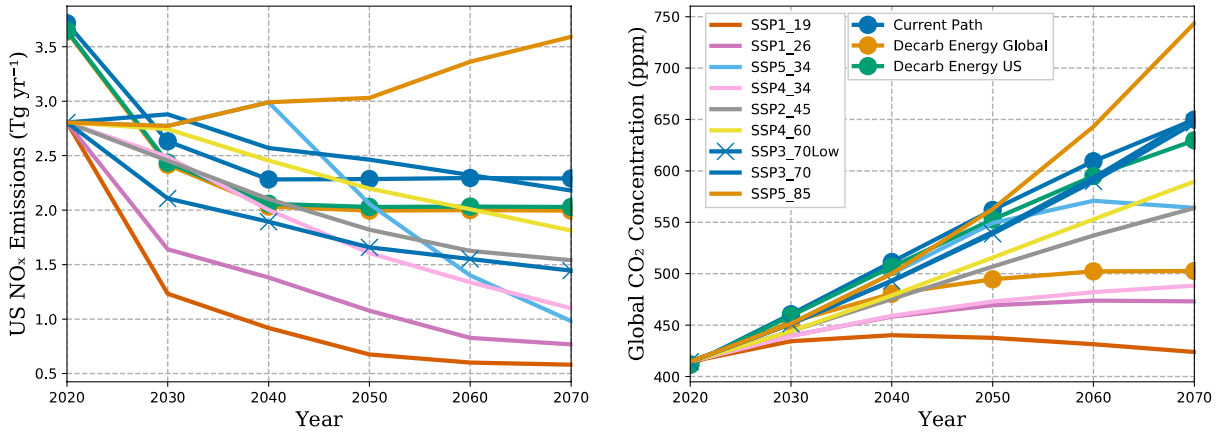

Figure S1. US nitrogen oxide (NO_x) emissions (left) and global CO_2 concentrations (right) in the indicated SSP and Energy-sector decarbonization scenarios. Decarb stands for decarbonization. Note that the Decarb Energy Global and Decarb Energy US scenarios have identical values for the US NO_x emissions.

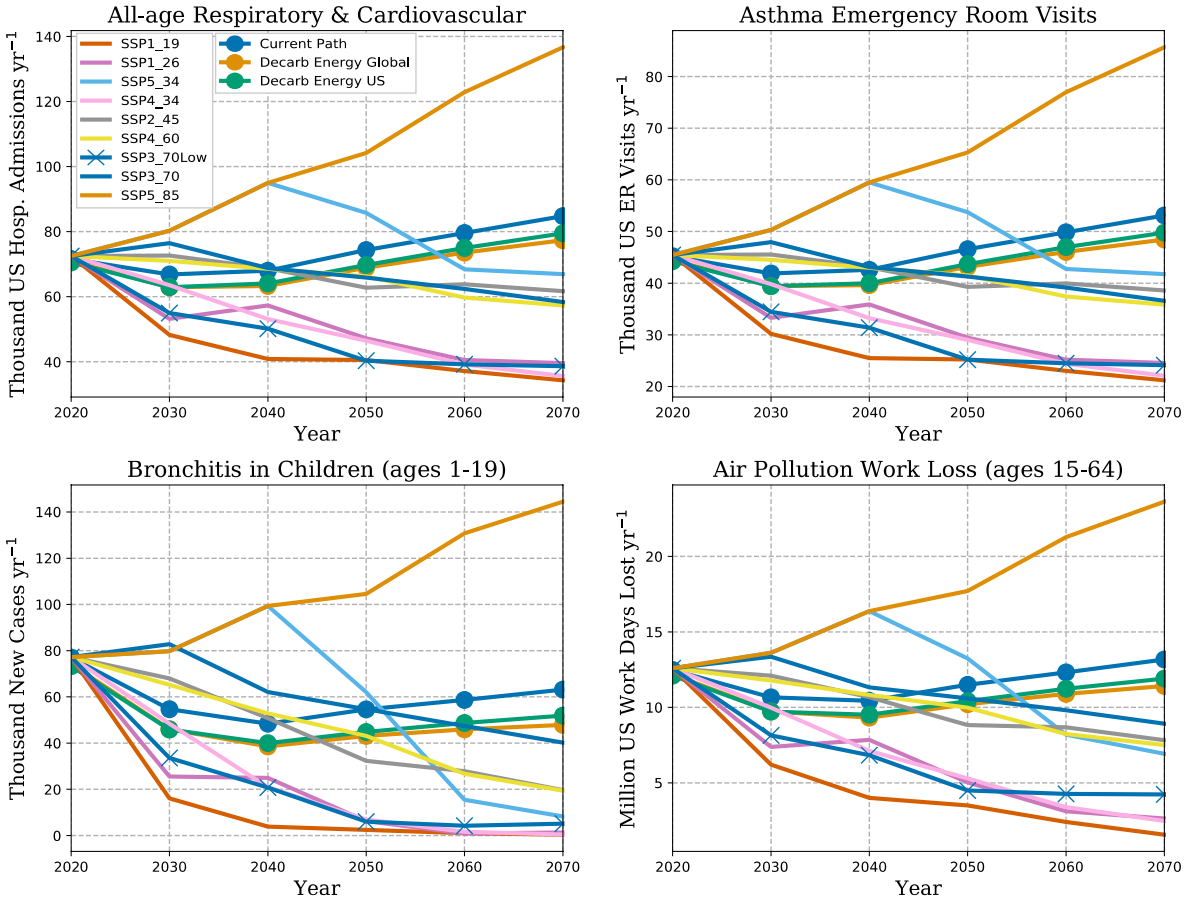

Figure S2. Hospital admissions, asthma-related Emergency Room Visits, child bronchitis cases, and work losses due to $PM_{2.5}$ exposure in the indicated scenarios. Health results shown here are those calculated using the log-linear models.

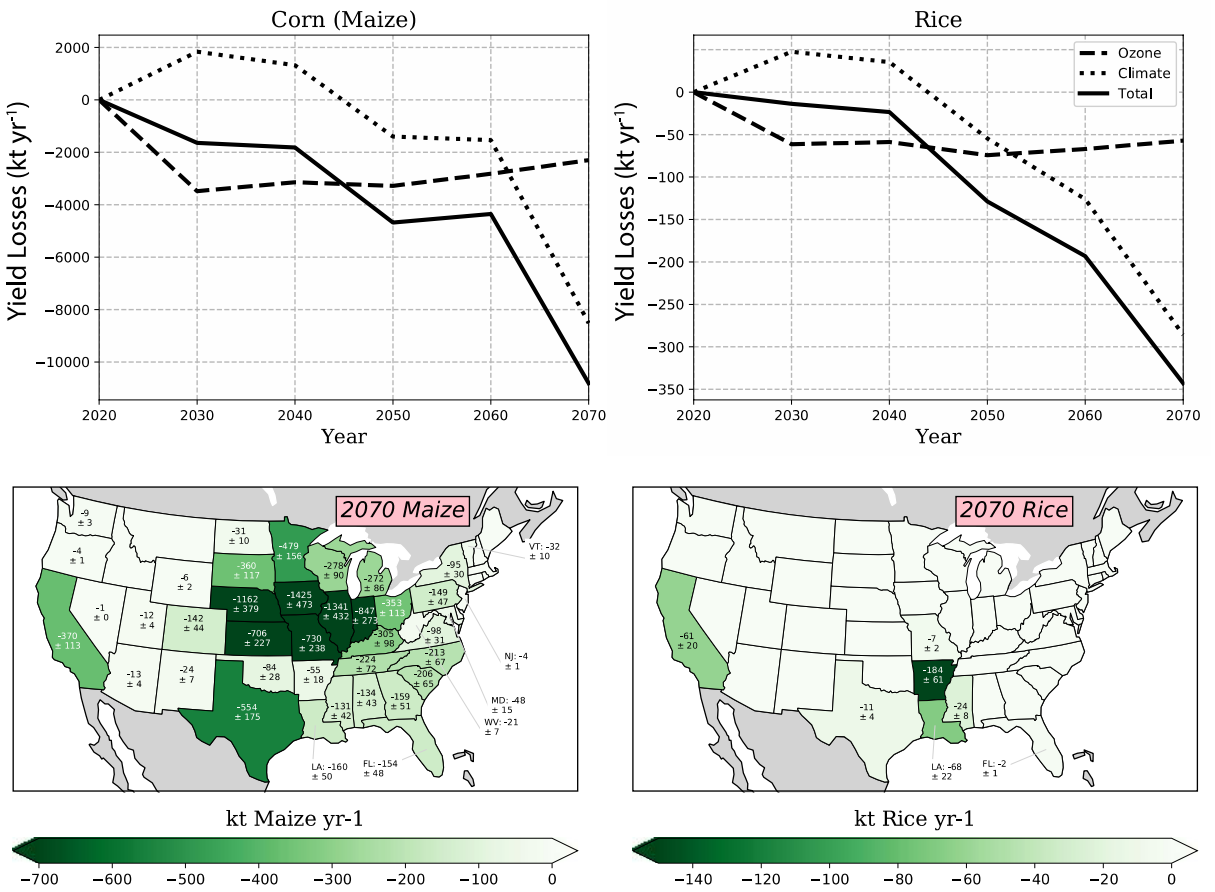

Figure S3. Total US yield changes for maize and rice under the 1.5°C scenario (SSP1_19) relative to the reference (SSP3_70). Maps are values for 2070 (bottom), while timeseries (top) separate impacts into those from ozone and climate where climate impacts include changes in temperature, precipitation and CO_2 concentrations.

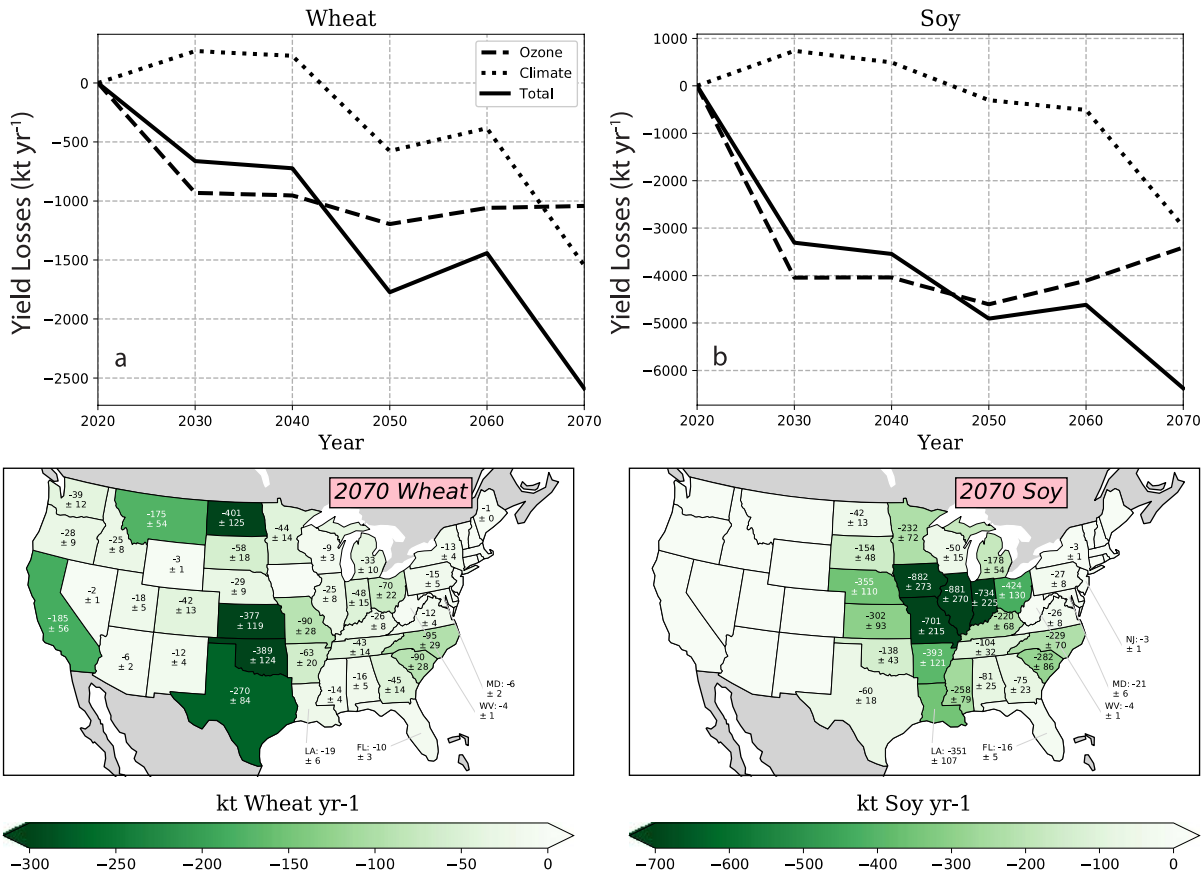

Figure S4. Avoided US yield losses as in Figure S3 but for soy and wheat under the 1.5°C scenario (SSP1_19) relative to the reference (SSP3_70) over time (top) and at the state level in 2070 (bottom). For timeseries, climate impacts include changes in temperature, precipitation and CO_2 concentrations.

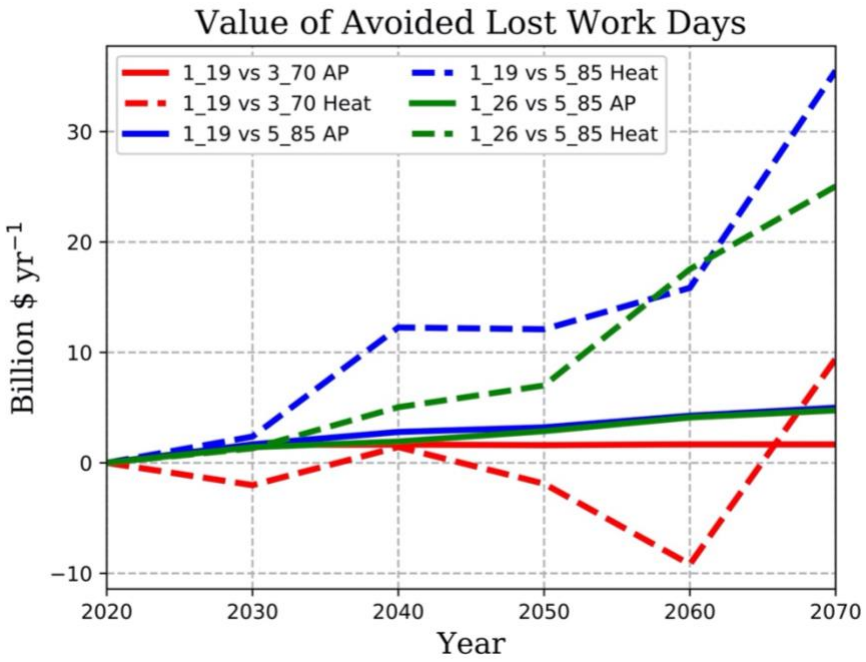

Figure S5. Valuation of avoided lost workdays in the US under the 1.5°C (SSP1_19) and 2°C (SSP1_26) scenarios relative to the lower (SSP3_70) and higher (SSP5_85) references without discounting of future damages. Lines labeled 'AP' are impacts due to air pollution ($PM_{2.5}$ exposure).

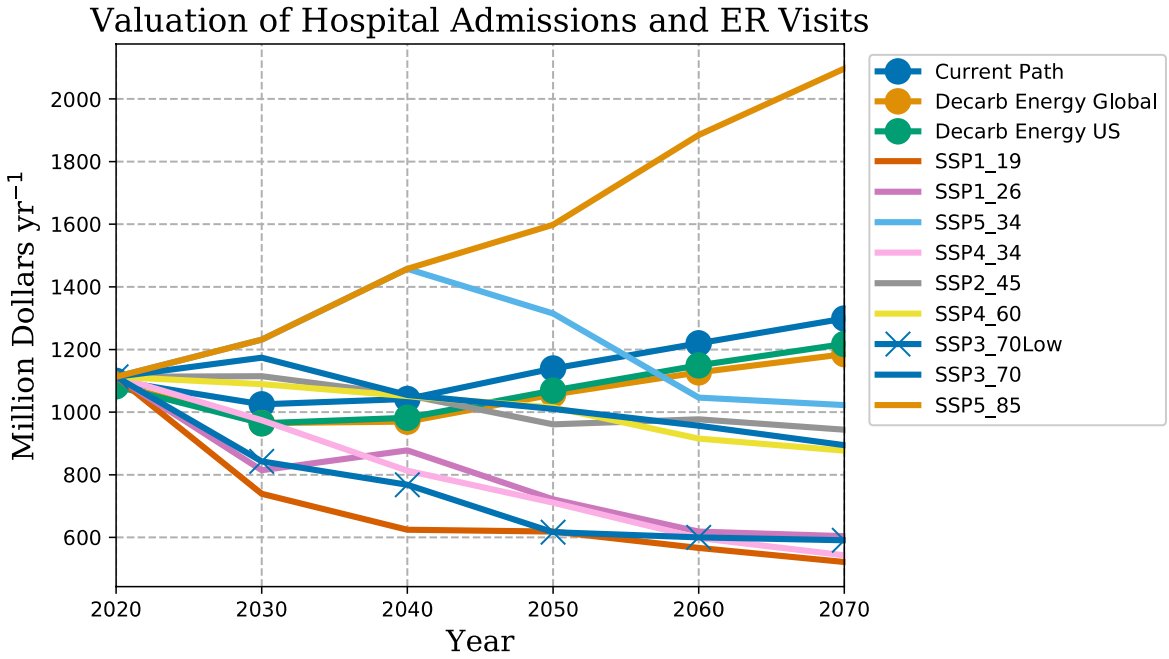

Figure S6. Valuation of avoided hospitalizations and Emergency Room (ER) visits due to $PM_{2.5}$ exposure in the US for the indicated scenarios without discounting of future damages.

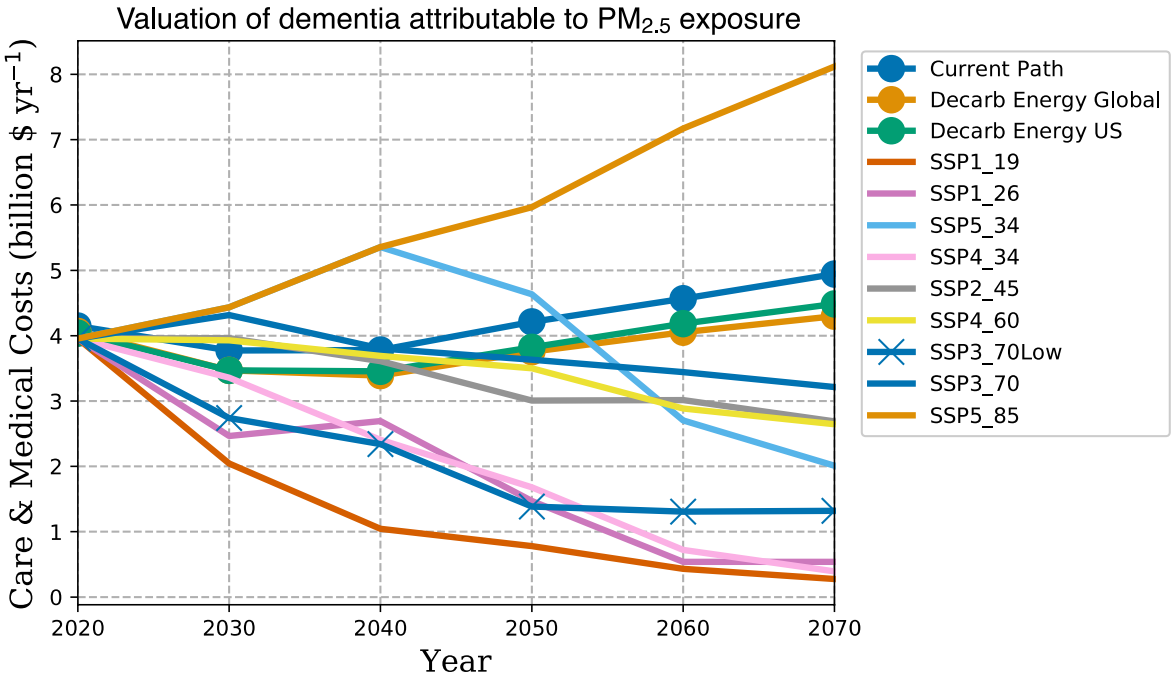

Figure S7. Valuation of avoided dementia incidences due to $PM_{2.5}$ exposure in the US for the indicated scenarios without discounting of future damages.

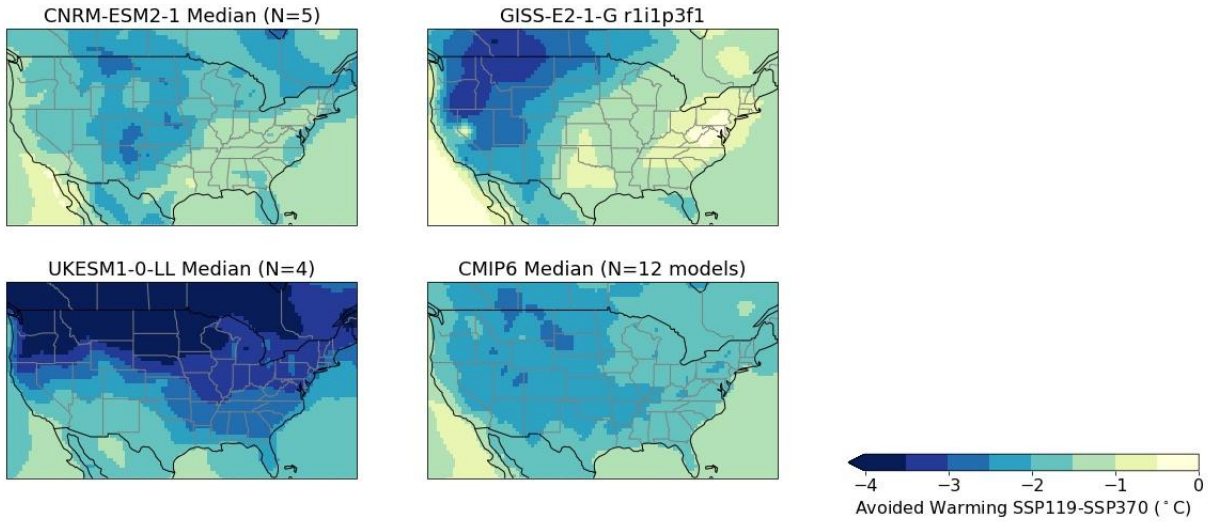

Figure S8. Surface temperature difference for June-August in the US in 2070 under the 1.5°C scenario (SSP1_19) relative to the lower reference (SSP3_70) in the GISS model used in this study and in two representative other CMIP6 models, a near-median model (CNRM-ESM2) and a high-end model (UKESM1). Values are means over 2065-2074 and are ensemble means for CNRM and UKESM. The CMIP6 median over 12 models with data for both scenarios available is also shown.

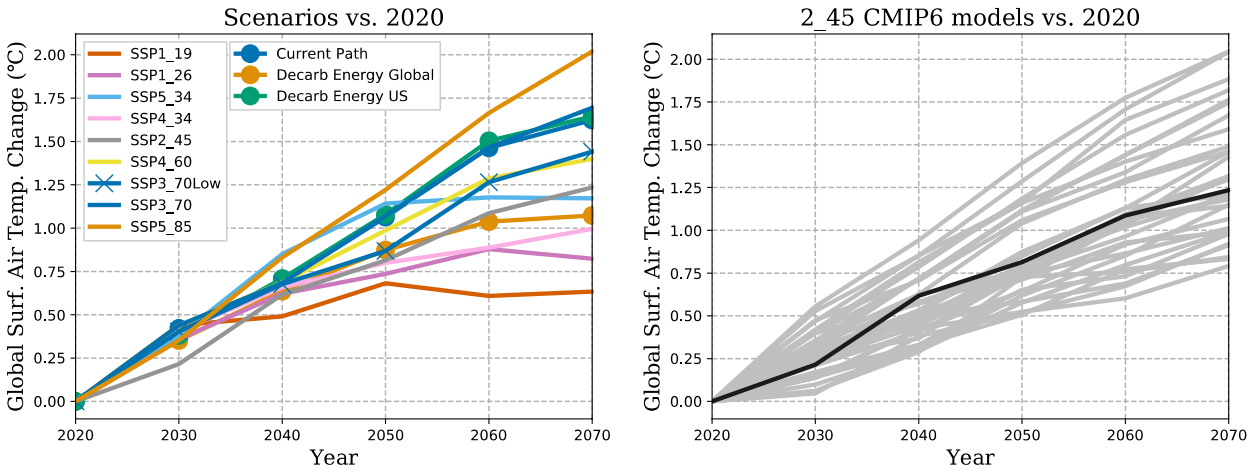

Figure S9. Global mean annual average surface air temperature change relative to the 2020 value in the indicated SSP and Energy-sector decarbonization scenarios (left) and under SSPSSP2_4.5 in the GISS-E2.1-G model used in this study (thick black line; ensemble mean of 5 members) and in all available CMIP6 models (gray lines) (right). Decarb stands for Decarbonization. Values are 10-yr running means for easier visualization.

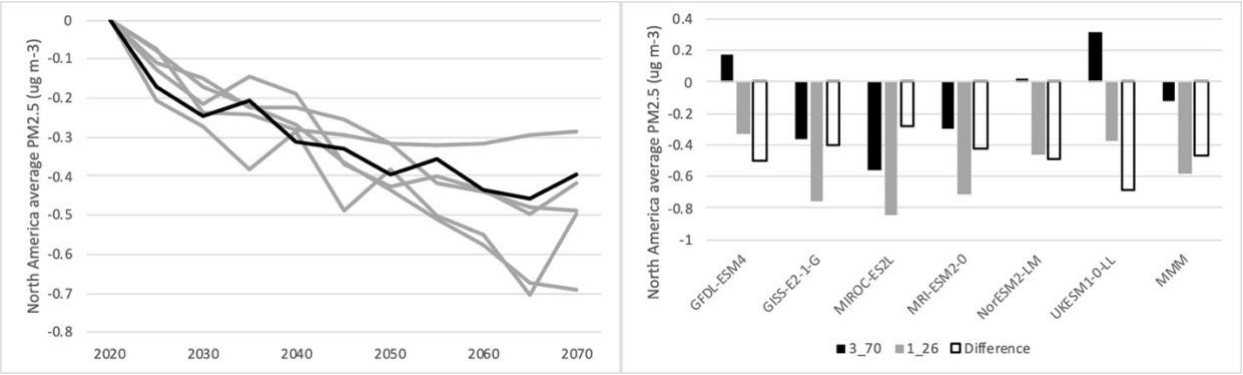

Figure S10. Differences in $PM_{2.5}$ between the 2°C-consistent (SSP1_26) and reference (SSP3_70) scenarios over North America during 2020-2070 as timeseries (left) and 2070 vs 2020 values for each scenario along with their difference (right). In the left panel, the GISS model is shown as a thick black line with the other CMIP6 models listed in the right panel shown in gray. In the right panel, MMM stands for multi-model mean. All values are 5-yr means.

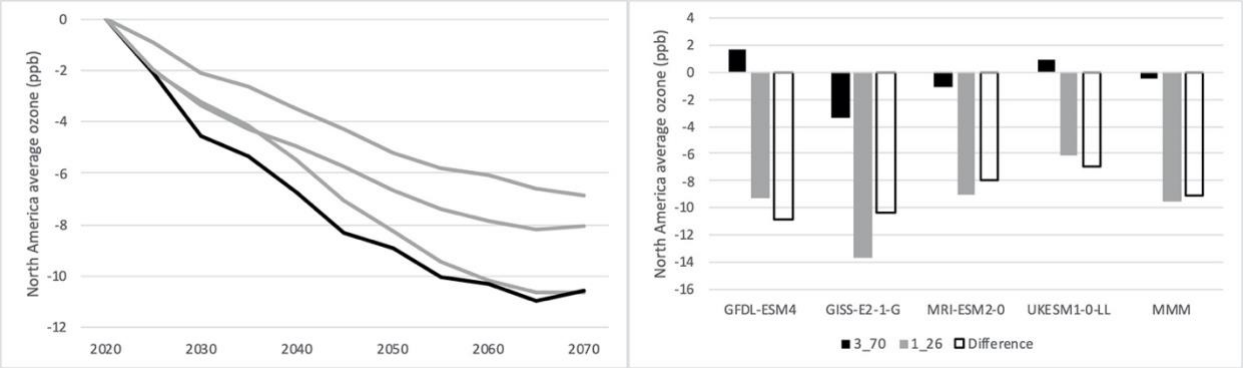

Figure S11. Differences in surface ozone between the 2°C-consistent (SSP1_26) and reference (SSP3_70) scenarios over North America during 2020-2070 as timeseries (left) and 2070 vs 2020 values for each scenario along with their difference (right). In the left panel, the GISS model is shown as a thick black line with the other CMIP6 models listed in the right panel shown in gray. In the right panel, MMM stands for multi-model mean. All values are 5-yr means.

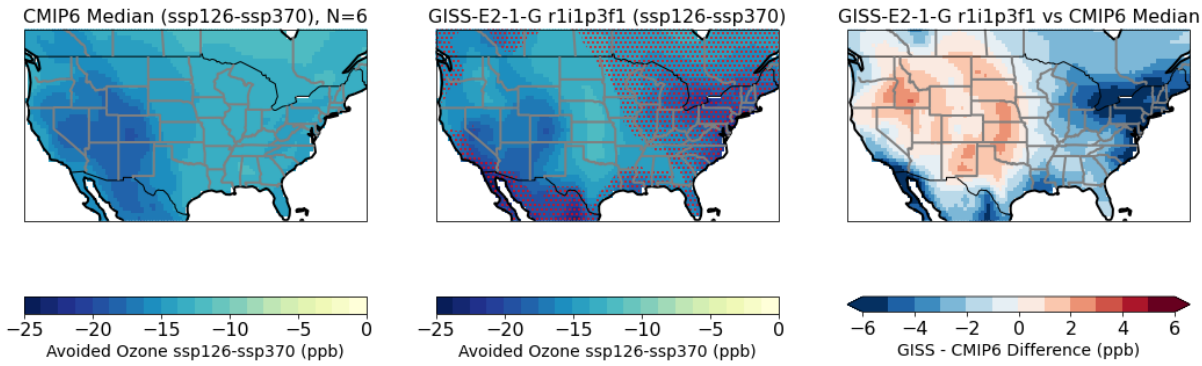

Figure S12. Annual average surface ozone difference in the US in 2070 under the 2°C scenario (SSP1_26) relative to the lower baseline (SSP3_70) for the CMIP6 median over 6 models (left; excluding GISS), for the GISS model used in this study (center), and their difference (right).

Supplementary References

Anenberg SC, Horowitz LW, Tong DQ, West JJ., An estimate of the global burden of anthropogenic ozone and fine particulate matter on premature human Mortality using atmospheric modeling, Env. Health Persp., 118, 1189–1195, 2010.

Basu, R., Gavin, L., Pearson, D., Ebisu, K. and Malig, B., Examining the association between apparent temperature and mental health-related emergency room visits in California. *American journal of epidemiology*, *187*(4), pp.726-735, 2018.

Burnett, R. T., et al., An integrated risk function for estimating the global burden of disease attributable to ambient fine particulate matter exposure, Environ. Health Perspect., 122, 397–403, 2014.

Carleton, T, M Delgado, M Greenstone, T Houser, S Hsiang, A Hultgren, et al., Valuing the global mortality consequences of climate change accounting for adaptation costs and benefits, University of Chicago Becker Friedman Institute for Economics Working Paper No. 2018–51, Chicago, USA, 2019. Available at SSRN: https://doi.org/10.2139/ssrn.3224365

Challinor, A. J., Watson, J., Lobell, D. B., Howden, S. M., Smith, D. R., & Chhetri, N., A meta-analysis of crop yield under climate change and adaptation. Nature Climate Change, 4(4), 287–291, 2014.

Chastek, B., Korrer, S., Nagar, S.P., Albers, F., Yancey, S., Ortega, H., Forshag, M. and Dalal, A.A., Economic burden of illness among patients with severe asthma in a managed care setting. *Journal of managed care & specialty pharmacy*, *22*, 848-861, 2016.

Center for International Earth Science Information Network - CIESIN - Columbia University, United Nations Food and Agriculture Programme - FAO, and Centro Internacional de Agricultura Tropical – CIAT, *Gridded Population of the World, Version 3 (GPWv3): Population Count Grid*. Palisades, NY: NASA Socioeconomic Data and Applications Center (SEDAC), 2005.

Fann, N., Coffman, E., Timin, B. and Kelly, J.T., The estimated change in the level and distribution of PM2. 5-attributable health impacts in the United States: 2005–2014. *Env. Res., 167*, 506-514, 2018.

Foure, J., Aguiar, A., Bibas, R., Chateau, J., Fujimori, S., Lefevre, J., Leimbach, M., Rey-Los-Santos, L. and Valin, H., Macroeconomic drivers of baseline scenarios in dynamic CGE models: review and guidelines proposal, *J. Global Econ. Anal., 5*, 28-62, 2020.

HCUPnet, Healthcare Cost and Utilization Project. Agency for Healthcare Research and Quality, Rockville, MD. https://hcupnet.ahrq.gov/.

Hoegh-Guldberg, O. *et al.*, in *Global warming of 1.5°C. An IPCC Special Report on the impacts of global warming of 1.5°C above pre-industrial levels and related global greenhouse gas emission pathways, in the context of strengthening the global response to the threat of climate change, sustainable development, and efforts to eradicate poverty*, P. Z. V. Masson-Delmotte, H. O. Pörtner, D. Roberts, J. Skea, P.R. Shukla, A. Pirani, W. Moufouma-Okia, C. Péan, R. Pidcock, S. Connors, J. B. R. Matthews, Y. Chen, X. Zhou, M. I. Gomis, E. Lonnoy, T. Maycock, M. Tignor, T. Waterfield, Ed. (Cambridge Univ Press, Cambridge, UK, 2018).

Honda, Y., Kondo, M., McGregor, G., Kim, H., Guo, Y. L., Hijioka, Y., et al., Heat-related mortality risk model for climate change impact projection, Environ. Health & Preventive Medicine, 19(1), 56–63, 2014.

Hsiang, S., Kopp, R., Jina, A., Hsiang, S., Kopp, R., Jina, A., et al., Estimating economic damage from climate change in the United States. Science, 356(6345), 1362–1369, 2017.

Hughes, BB, et al., Projections of global health outcomes from 2005 to 2060 using the International Futures integrated forecasting model, Bull. World Health Organ., 89: 478-486, 2011.

International Energy Agency (IEA), Energy Technology Perspectives. 2012 - Pathways to a Clean Energy System, OECD/IEA, Paris; http://www.iea.org/Textbase/nptoc/etp2012toc.pdf

International Institute of Applied Systems Analysis (IIASA) ECLIPSE v5a data, http://www.iiasa.ac.at/web/home/research/researchPrograms/air/Global_emissions.html; accessed July 2017.

Jerrett, M., et al., Long-term ozone exposure and mortality, New Engl. J. Med., 360, 1085–95, 2009.

Jones, B., and O'Neill, B. C., Spatially explicit global population scenarios consistent with the Shared Socioeconomic Pathways, Environ. Res. Lett. 11 084003, 2016.

KC, S., and W. Lutz, The human core of the shared socioeconomic pathways: Population scenarios by age, sex and level of education for all countries to 2100, Global Env. Change, 42, 181-192, 2017.

Lee, M., Nordio, F., Zanobetti, A., Kinney, P., Vautard, R., & Schwartz, J., Acclimatization across space and time in the effects of temperature on mortality: A time-series analysis, Environ. Health, 13(1), 1–9, 2014.

Livingston, G., Huntle, J., Sommerlad, A., Ames, D., Ballard, C., Banerjee, S., Brayne, C., Burns, A., Cohen-Mansfield, J, and Cooper, C., Dementia prevention, intervention, and care: 2020 report of the Lancet Commission. *The Lancet*, 396**,** 413-446, 2020.

Malley CS, Henze DK, Kuylenstierna JCI, Vallack HW, Davila Y, Anenberg SC, et al., Updated global estimates of respiratory mortality in adults ≥ 30 years of age attributable to long-term ozone exposure, Env. Health Persp., 125, 087021, 2017.

Markandya, A. *et al.*, Health co-benefits from air pollution and mitigation costs of the Paris Agreement: a modelling study. *Lancet Planetary Health* **2**, E126-E133 (2018).

McCollum, D. L. *et al.*, Energy investment needs for fulfilling the Paris Agreement and achieving the Sustainable Development Goals. *Nature Energy* **3**, 589-599 (2018).

Myers, S. S., *et al.*, Increasing CO2 threatens human nutrition. *Nature* **510**, 139-142 (2014).
Nasari, M.M., Szyszkowicz, M., Chen, H., Crouse, D., Turner, M.C., Jerrett, M., Pope, C.A., Hubbell, B., Fann, N., Cohen, A. and Gapstur, S.M., A class of non-linear exposure-response models suitable for health impact assessment applicable to large cohort studies of ambient air pollution. *Air Quality, Atmosphere & Health*, *9*(8), 961-972, 2016.

Nijsse, F.J., Cox, P.M. and Williamson, M.S., Emergent constraints on transient climate response (TCR) and equilibrium climate sensitivity (ECS) from historical warming in CMIP5 and CMIP6 models, Earth Sys. Dyn., 11, 737-750, 2020.

Nordhaus, W., A question of balance, Yale University Press, New Haven, CT, USA, 2008.

Ostro, B. D., Air pollution and morbidity revisited: a specification test. *J. Environ. Econ. & Mgmt.*, 14**,** 87-98, 1987.

Rao, S., Klimont, Z., Smith, S.J., Van Dingenen, R., Dentener, F., Bouwman, L., Riahi, K., Amann, M., Bodirsky, B.L., van Vuuren, D.P. and Reis, L.A., Future air pollution in the Shared Socio-economic Pathways, *Global Environmental Change*, *42*, 346-358, 2017.

Ru, M., M. Brauer, J.-F. Lamarque, D. Shindell, Exploration of the global burden of dementia attributable to PM2.5: what do we know based on current evidence? *GeoHealth*, doi:10.1029/2020GH000356 (2021).

Sarofim, M. C., Saha, S., Hawkins, M. D., Mills, D. M., Hess, J., Horton, R., et al., Temperature-related death and illness, in "The impacts of climate change on human health in the United States: A scientific assessment", pp. 43–68, Washington, DC: US Global Change Research Program, 2016.

Sellers, S., Cause of death variation under the sharedsocioeconomic pathways, Climatic Change, 163, 559-577, 2020.

Seltzer, K. M., D. T. Shindell, G. Faluvegi, L. T. Murray, Evaluating Modeled Impact Metrics for Human Health, Agriculture Growth, and Near-Term Climate. Journal of Geophysical Research-Atmospheres, 122, 13506-13524, 2017.

Seltzer, K., D. Shindell, C. Malley, Measurement-based assessment of health burdens from long-term ozone exposure in the United States, Europe, and China, Env. Res. Lett., 13, 104018, 2018.

Shaddick, G., Thomas, M.L., Amini, H., Broday, D., Cohen, A., Frostad, J., Green, A., Gumy, S., Liu, Y., Martin, R.V. and Pruss-Ustun, A., Data integration for the assessment of population exposure to ambient air pollution for global burden of disease assessment. Env. Sci. Tech., 52, 9069-9078, 2018.

Sherwood, S.C., Webb, M.J., Annan, J.D., Armour, K.C., Forster, P.M., Hargreaves, J.C., Hegerl, G., Klein, S.A., Marvel, K.D., Rohling, E.J. and Watanabe, M., An assessment of Earth's climate sensitivity using multiple lines of evidence, Rev. Geophys., 58, p.e2019RG000678, 2020.

Shindell, D., J. C. I. Kuylenstierna, E. Vignati, R. Dingenen, M. Amann, Z. Klimont, S. C. Anenberg, N. Muller, G. Janssens-Maenhout, F. Raes, J. Schwartz, G. Faluvegi, L. Pozzoli, K. Kupiainen, L. Höglund-Isaksson, L. Emberson, D. Streets, V. Ramanathan, K. Hicks, K. Oanh, G. Milly, M. Williams, V. Demkine, and D. Fowler, Simultaneously mitigating near-term climate change and improving human health and food security, Science, 335, 183-189, 2012.

Shindell, D., G. Faluvegi, P. Kasibhatla, R. Van Dingenen, Spatial patterns of crop yield change by emitted pollutant, Earth's Future, 7, 101-112, 2019.

Shindell, D., C. J. Smith, Climate and air-quality benefits of a realistic phase-out of fossil fuels, Nature, 573, 408-411, 2019.

Spadaro, J.V., Kendrovski, V. and Martinez, G.S., Achieving health benefits from carbon reductions: Manual for CaRBonH calculation tool, World Health Organization, Geneva, 2018. (available at: https://core.ac.uk/reader/189891440)

Stanaway et al., Global, regional, and national comparative risk assessment of 84 behavioural, environmental and occupational, and metabolic risks or clusters of risks for 195 countries and territories, 1990–2017: A systematic analysis for the Global Burden of Disease Study, Lancet, 1923–1994, 2018.

Stohl, A., Aamaas, B., Amann, M., Baker, L. H., Bellouin, N., Berntsen, T. K., Boucher, O., Cherian, R., Collins, W., Daskalakis, N., Dusinska, M., Eckhardt, S., Fuglestvedt, J. S., Harju, M., Heyes, C., Hodnebrog, Ø., Hao, J., Im, U., Kanakidou, M., Klimont, Z., Kupiainen, K., Law, K. S., Lund, M. T., Maas, R., MacIntosh, C. R., Myhre, G., Myriokefalitakis, S., Olivié, D., Quaas, J., Quennehen, B., Raut, J.-C., Rumbold, S. T., Samset, B. H., Schulz, M., Seland, Ø., Shine, K. P., Skeie, R. B., Wang, S., Yttri, K. E., and Zhu, T.: Evaluating the climate and air quality impacts of short-lived pollutants, Atmos. Chem. Phys. 15, 10529–10566, 2015.

Tebaldi, C., & Lobell, D., Estimated impacts of emission reductions on wheat and maize crops. *Climatic Change*, *146*(3-4), 533-545, 2018.

Turner, M. C., et al., Long-term ozone exposure and mortality in a large prospective study, Am. J. Respir. Crit. Care Med., 193, 1134–42, 2016.

U.S. Environmental Protection Agency. 1997. *The Benefits and Costs of the Clean Air Act 1970-1990.* Prepared for Congress by Office of Air and Radiation and Office of Policy, Planning and Evaluation. October 1997.

USEPA. 2015. *Environmental Benefits Mapping and Analysis Program–Community Edition (BenMAP-CE)* [Online]. US Environmental Protection Agency. [Accessed July 30, 2020].

USGCRP, Climate Science Special Report: Fourth National Climate Assessment, Volume I. Wuebbles, D.J., D.W. Fahey, K.A. Hibbard, D.J. Dokken, B.C. Stewart, and T.K. Maycock, Eds. U.S. Global Change Research Program, Washington, DC, USA, 470 pp., 2018.

Van Dingenen, R., Dentener, F. J., Raes, F., Krol, M. C., Emberson, L., & Cofala, J., The global impact of ozone on agricultural crop yields under current and future air quality legislation. *Atmospheric Environment*, *43*, 604–618, 2009.

Van Vuuren, D.P., Stehfest, E., Gernaat, D.E., Doelman, J.C., Van den Berg, M., Harmsen, M., de Boer, H.S., Bouwman, L.F., Daioglou, V., Edelenbosch, O.Y. and Girod, B., 2017. Energy, land-use and greenhouse gas emissions trajectories under a green growth paradigm. Global Environmental Change, 42, 237-250, 2017.

Vodonos, A., Abu Awad, Y., Schwartz, J., The concentration-response between long-term PM2.5 exposure and mortality; A meta-regression approach, Environ Res, 166, 677-689, 2018.

Vohra, K., Vodonos, A., Schwartz, J., Marais, E.A., Sulprizio, M.P., Mickley, L.J., Global mortality from outdoor fine particle pollution generated by fossil fuel combustion: Results from GEOS-Chem, Env. Res., https://doi.org/10.1016/j.envres.2021.110754, 2021.

Viscusi WK, Aldy JE, The Value of a Statistical Life: A Critical Review of Market Estimates Throughout the World. J. Risk Uncert. 27:5–76, 2003.

Wang, X., Mauzerall, D.L., Characterizing distributions of surface ozone and its impact on grain production in China, Japan and South Korea: 1990 and 2020, Atmospheric Environment, 38, 4383–4402, 2004.

Weinberger, K. R., Haykin, L., Eliot, M. N., Schwartz, J. D., Gasparrini, A., & Wellenius, G. A., Projected temperature-related deaths in ten large US metropolitan areas under different climate change scenarios, Environ. Int., 107, 196–204, 2017.

Williams, J. H. *et al.*, Carbon-neutral pathways for the United States. *AGU Advances* **2**, e2020AV000284 (2021).

Wimo, A., Guerchet, M., Ali, G. C., Wu, Y. T., Prina, A. M., Winblad, B., Jonsson, L., Liu, Z. and Prince, M., The worldwide costs of dementia 2015 and comparisons with 2010, Alzheimers Dement., 13, 1-7, 2017.

Yohe, G. W., Characterizing transient temperature trajectories for assessing the value of achieving alternative temperature targets. *Climatic Change* **145**, 469-479 (2017).

Zhang, Y., D. Shindell, Costs from labor losses due to extreme heat in the United States attributable to climate change. *Climatic Change*, 164:35, 2021.

Zhao, C., Liu, B., Piao, S., Wang, X., Lobell, D. B., Huang, Y., ... & Durand, J. L., Temperature increase reduces global yields of major crops in four independent estimates. *Proceedings of the National Academy of Sciences*, *114*(35), 9326-9331, 2017.